J. Fluid Mech. (2014), *vol.* 758, *pp.* 621–654.
doi:10.1017/jfm.2014.551

Inertial wave rays in rotating spherical fluid domains

Anna Rabitti[1,†] **and Leo R. M. Maas**[1]

[1]Department of Physical Oceanography, NIOZ Royal Netherlands Institute for Sea Research, PO Box 59, 1790 AB Texel, The Netherlands

(Received 17 March 2014; revised 15 July 2014; accepted 17 September 2014; first published online 10 October 2014)

The behaviour of inertial waves in a rotating spherical container, filled with homogeneous fluid, is here investigated by means of a three-dimensional ray tracing algorithm, in a linear, inviscid framework. In particular, the classical, two-dimensional association between regular modes and periodic trajectories is addressed here for the first time in a fully three-dimensional setting. Three-dimensional, repelling periodic trajectories are found and classified on the basis of the associated frequency and spatial structure, although associated frequencies are hardly reconcilable to Bryan's (*Proc. R. Soc. Lond.*, vol. 45, 1889, pp. 42–45) classical solutions for inertial waves in the sphere. The normalized squared frequency $\omega^2 = 1/2$ appears to divide the frequency range into two different trajectory regimes, where critical latitudes play a different role. Chaotic orbits are not found, as expected, while invariant, non-domain-filling orbits (whispering gallery modes) constitute the majority of the trajectories in the sphere. From ray tracing alone, the wavefield is still far from being completely reconstructed, and a study performed in such a simplified setting is clearly far from any realistic application, however, it appears that three-dimensional ray dynamics constitutes a valid approach to infer information on the spectrum and regularity properties of a system, and is then able to bring new insight in a variety of fundamental problems of geophysical and astrophysical relevance, once its power and limitations have been recognized.

Key words: general fluid mechanics, internal waves, waves in rotating fluids

1. Introduction

Internal waves have long been the subject of numerous studies, motivated by their fundamental character and the variety of possible applications. In fact, they are present in all stratified and/or rotating fluids, including astrophysical and geophysical fluids, where they are considered a key mechanism contributing to internal mixing and dynamics (Dintrans, Rieutord & Valdettaro 1999; Ogilvie & Lin 2004; Wunsch & Ferrari 2004; van Haren & Gostiaux 2012).

Interestingly, internal gravity waves and internal inertial (or gyroscopic) waves share many aspects in their dynamics and mathematical description, irrespective of the nature of the acting restoring force (gravity or Coriolis acceleration, respectively).

† Email address for correspondence: anna.rabitti@nioz.nl

In this work we will restrict ourselves to the study of pure inertial waves propagating in a homogeneous fluid, but it follows that results that are valid for one type of internal waves are generally of relevance for the whole class.

Despite the recent progress, especially regarding high-resolution numerical models (Baruteau & Rieutord 2013; Nurijanyan, Bokhove & Maas 2013; Favier *et al.* 2014), one key challenge is still limiting our ability to satisfyingly comprehend propagating internal waves: their hyperbolic character is hardly reconcilable with their confinement to a fully enclosed domain, resulting, for an arbitrarily shaped container, in a paradigmatic, mathematically ill-posed Poincaré problem (see Cartan (1922) and, for example, Stewartson & Rickard (1969) and Rieutord, Georgeot & Valdettaro (2000) for the case of a spherical shell container).

Owing to this difficulty, regular, analytic solutions (smooth functions, finite in all points of the domain) for inertial wave problems in enclosed domains are known only for homogeneous fluids contained in exceptionally symmetric geometries, such as for two dimensions, the rectangle and the circle (see for example Barcilon 1968), and for the three-dimensional case, the axial cylinder (Lord Kelvin 1880*b*; Høiland 1962), the axial ellipsoid (Kudlick 1966) and the full sphere (Bryan 1889; Zhang *et al.* 2001). Quasi-analytical methods have also been used to compute regular inertial wavefields in the case of an untilted rectangular parallelepiped (Maas 2003; Nurijanyan *et al.* 2013).

In order to study the propagation and the properties of internal waves in differently shaped, two-dimensional domains, where analytical solutions are unavailable, ray theory has been developed (Whitham 1960, 1974). When the amplitude of the propagating wave is assumed to be slowly varying in space and time compared with variations in the phase function and in the conditions of the supporting medium, it is possible to treat these slowly modulated waves as nearly planar waves, and solve the original equation in the short wavelength limit, often referred to as the Wentzel–Kramers–Brillouin–Jeffreys (WKBJ) approximation. This simplified approach is not only valid for describing internal waves, but has been also frequently used to describe the dynamics of inviscid, short surface gravity waves. Since surface waves are exponentially trapped to the surface, they propagate strictly in the horizontal plane and their velocity potential is described by a Helmholtz equation (Maas 2005). It follows that for waves that are short compared with the scale over which water depth and radius of curvature of the wall change, WKBJ theory determines approximate solutions to the Helmholtz equation. Short surface waves propagating over flat bottoms, as well as two-dimensional inertial waves, trace then straight ray paths in real space, similar to the paths traced by balls bouncing elastically on a billiard.

In the case of internal waves, the tracing is performed by following the propagation of corresponding energy rays, whose inclination with respect to the restoring force direction (gravity or rotation axis) is determined by the ratio of the perturbing frequency and a frequency representing the local environmental conditions (density stratification and/or rotation). Rays are then supposed to provide a (partial) view on the energy distribution in the domain and on the regularity of the associated wavefield (or the lack of it).

The correspondence between characteristic curves of the original partial differential equation and approximated, geometrical, internal wave energy rays is not trivial (Eckart 1960). However, the correspondence is exact for two-dimensional internal waves, propagating obliquely in the vertical plane, under a wide range of circumstances (Harlander & Maas 2006). Remarkably, despite the strong assumptions underlying ray tracing, this investigation tool has been proven useful even in applied, realistic cases, where the ray approach has been tested against laboratory observations

(Maas *et al.* 1997; Manders & Maas 2004; Hazewinkel *et al.* 2008; Hazewinkel, Grisouard & Dalziel 2010), numerical simulations (Dintrans *et al.* 1999; Rieutord, Georgeot & Valdettaro 2001) or analysed in a selection of geophysical applications (Broutman, Rottman & Eckermann 2004); in all of these cases, ray tracing has been generally recognized to provide a unique contribution to the understanding of the spatial structure and spectra of internal wavefields.

As we have seen, in the short wavelength limit, surface waves over flat-bottom basins also follow straight ray paths, which on non-trivially shaped domains are either periodic, invariant (never closing orbits, infinitely repeating the same spatial structure, while being slightly offset) or chaotic (Berry 1981; Kudrolli, Abraham & Gollub 2001). While the periodic paths, and the invariant modes, have measure zero amongst the chaotic paths, they dominate the response of higher modes, and are therefore referred to as scars (Heller 1984). By contrast, three different types of ray trajectories are observed when internal waves are obliquely propagating in two-dimensional vertical domains (John 1941; Maas & Lam 1995; Dintrans *et al.* 1999). A trajectory can be closed and periodic after a finite number of reflections on the boundary. A trajectory can be ergodic and plane filling, or, lastly, a trajectory can be attracting, meaning that there exist one or more limit cycles towards which neighbouring trajectories are attracted.

The first two kinds of trajectories are usually associated with the presence of regular modes in the system and with a dense spectrum, such as occurs in the untilted rectangular domain, or the circle (Barcilon 1968). In these domains, periodic ray trajectories occur at frequencies corresponding to eigenfrequencies of the system, while rays corresponding to other frequencies fill the fluid domain ergodically.

In addition to being dense, the spectrum of two-dimensional regular systems is also infinitely degenerate (Münnich 1996): consequently, for each eigenfrequency, an infinite number of periodic orbits exist, that together cover the whole domain.

By contrast, the occurrence of attracting trajectories (‘wave attractors’) is the signature of the singular nature of solutions. Attractors can be observed in all ‘symmetry breaking’ domains (e.g. trapezoidal, parabolic, tilted rectangular or annular domains), so called because the reflecting walls are not all parallel nor perpendicular to the restoring force. In this case, energy is collected from the whole basin and trapped onto the asymptotically closed trajectories (the attractors), focusing towards smaller and smaller scales until wave breaking, other nonlinearities and viscous effects come into play (Maas & Lam 1995; Ogilvie 2005; Harlander & Maas 2007; Hazewinkel *et al.* 2008; Scolan, Ermanyuk & Dauxois 2013). Exceptionally, in the case of a toroidal shell in the limit of long radius, analytical solutions are also known for modes focused along the emerging attractors (Rieutord, Valdettaro & Georgeot 2002).

Once these two-dimensional ray tracing results were shown to be robust, an increasing interest in the three-dimensional representation of internal waves in three-dimensional containers has obviously arisen. In order to extend ray tracing to three-dimensional, curved domains, however, a further consideration has to be made: considering the WKBJ limit, and its assumption that the wavelength needs to be short compared with the spatial scale of boundary variations, the propagating perturbation bouncing from a curved boundary is further idealized as if reflecting from a local tangent plane (see also Baines 1971). Given these approximations, a three-dimensional ray tracing algorithm can then be developed and, in three-dimensional containers, rays can be geometrically traced and their behaviour studied (Manders & Maas 2004; Maas 2005; Hazewinkel, Maas & Dalziel 2011; Rabitti & Maas 2013).

In analogy with the two-dimensional correspondence, in the presence of internal wave attractors, a relation between wave rays and energy paths in three-dimensional geometries is supported by recent numerical work in a tidal channel (Drijfhout & Maas 2007) and by laboratory experiments performed in a non-centrally forced paraboloidal basin filled with a uniformly stratified fluid (Hazewinkel *et al.* 2011).

However, all three-dimensional studies so far have been devoted to the investigation of symmetry-breaking geometries, because of the possibly crucial role played by wave attractors in the energy distribution in the basin, and consequently in relevant geophysical and astrophysical analogous contexts. But how robust is the analogy between two- and three-dimensional ray tracing, and how tight is the association between ray behaviour and properties of the underlying wavefield?

In this study, the case of pure inertial waves in a homogeneous fluid contained in a three-dimensional, uniformly rotating full sphere is considered. For this setting, in fact, three-dimensional analytic solutions are known (Bryan 1889; Zhang *et al.* 2001). The ray tracing algorithm is the same as used by Rabitti & Maas (2013) in a rotating spherical shell: it can be adopted here with little changes. Questions we wish to raise are as follows. Do three-dimensional periodic inertial wave ray trajectories ('scars') exist in a spherical domain? Is the classical, two-dimensional association between regular modes and periodic trajectories still valid in three dimensions? How do the frequencies associated with periodic trajectories relate to the analytical spectrum of inertial waves in a sphere (Bryan 1889)? And to experimental observations? How can real space trajectories in the sphere be classified in an appropriate phase space, in terms used in the description of quantum chaos (Berry 1987)?

The plan of this paper is as follows. Methodologies are presented in § 2: analytical solutions for inertial waves in a sphere are briefly recalled in § 2.1, a WKBJ approach is sketched in § 2.2, whereas the geometrical formulation of the ray tracing algorithm is described in § 2.3. A short review on the relations between ray trajectories, eigenmodes and physical fields of a system is presented in § 2.4. Results from the application of the ray tracing algorithm are presented in § 3. Three-dimensional periodic trajectories are found in the full rotating sphere, and a first attempt at classifying these orbits is presented, based on the associated frequency and corresponding spatial structure. In § 3.9 the different class of real space trajectories are analysed in their corresponding phase space (Berry 1981, 1987), where successive reflections are followed using the polar angle at subsequent reflection points and the angle of incidence of the ray relative to the normal at the same reflection point (Nöckel 1997).

Even if a general picture is far from being complete, the significance of periodic (and of non-periodic) orbits is discussed in § 4, both with respect to previous two-dimensional comparisons in literature as well as to wavefield reconstruction. A summary of the findings is given in § 5, while comparisons with previous experimental studies and concluding remarks are presented in § 6.

2. Inertial waves in the sphere: methods

2.1. *Analytical solutions*

In a homogeneous, inviscid, uniformly rotating fluid, momentum and mass conservation lead to the linearized equations of motion for small amplitude perturbations of velocity $\boldsymbol{u}$ and pressure p:

$$\left.\begin{aligned} \frac{\partial \boldsymbol{u}}{\partial t} + \boldsymbol{e}_z \times \boldsymbol{u} &= -\boldsymbol{\nabla} p \\ \boldsymbol{\nabla} \cdot \boldsymbol{u} &= 0 \end{aligned}\right\} \tag{2.1}$$

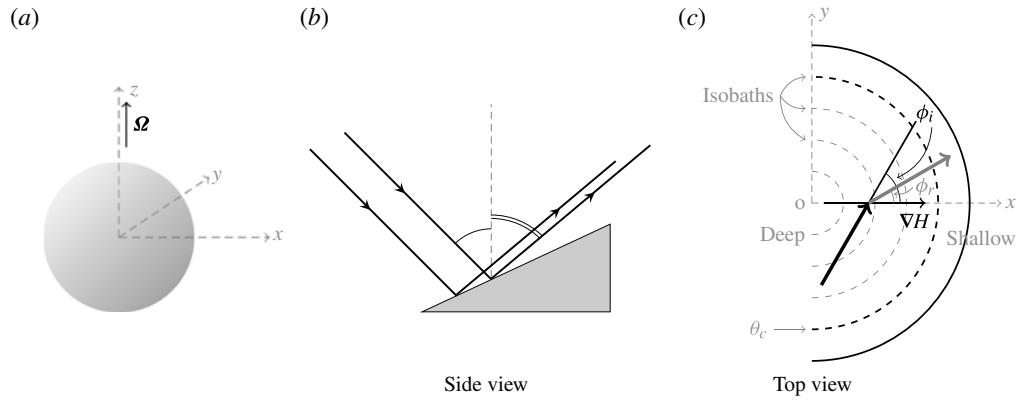

FIGURE 1. (*a*) Rotating fluid sphere in the Cartesian coordinate framework. (*b*) Side and (*c*) top view of a short internal wavepacket that reflects subcritically (see the text for explanation) from a sloping bottom. In (*c*) the rotation axis (coinciding with the z-axis) is pointing towards the reader. Modified after Maas (2005). In (*b*), note that while incident and reflected rays lie on the same cone (whose angle θ with the vertical is fixed by the perturbing frequency), the angle with the vertical can differ in a projection on the vertical plane perpendicular to the slope at the point of reflection. In (*c*), reflecting waves refract, instantaneously changing the horizontal propagation direction from ϕ_i to ϕ_r. Here θ_c denotes the critical latitude, where the bottom slope equals the wave ray inclination.

where the Coriolis parameter $(2\Omega)^{-1}$ is used as time scale, and the fluid is rotating at rate Ω oriented parallel to the vertical z direction (unit vector $\boldsymbol{e}_z$, see figure 1*a*). When all fields are assumed to have a $\mathrm{e}^{-\mathrm{i}\omega t}$ time dependency, the problem can then be conveniently cast in terms of pressure only and described by the Poincaré equation (Cartan 1922):

$$p_{xx} + p_{yy} - \lambda^2 p_{zz} = 0. \tag{2.2}$$

with

$$\lambda^2 = \frac{1-\omega^2}{\omega^2}. \tag{2.3}$$

Propagating inertial waves exist in the frequency range $0 < \omega < 1$, when the Poincaré equation is hyperbolic. Note that, compared with two-dimensional internal wave problems, the additional second-order horizontal derivative lends some aspects of an elliptic problem (such as surface wave problems) to the Poincaré equation. When the fluid is fully confined, the boundary condition for internal waves requires vanishing of the normal velocity component at the container's walls. In the case of a spherical container, this means vanishing of the radial velocity component $u_r = 0$ at $r = 1$, where the sphere's radius is used as spatial scale. This implies that the pressure field has to obey oblique derivative boundary conditions, that prohibits finding exact analytical solutions in arbitrarily shaped containers. However, when the container possesses some regularity and symmetry, the Poincaré problem is solvable. This happens, for instance, when the sidewalls of the container are parallel to the rotation axis and the vertical dependency can be split off, leaving a Helmholtz equation to be satisfied in the horizontal plane (Maas 2003).

In the case of the spherical container, it was shown by Bryan (1889) that a transformation of (2.2) from a cylindrical coordinate system (ϕ, r, z), initially

chosen because geostrophic contours on the sphere correspond to circles of constant cylindrical radii at fixed distances from the rotation axis, to a pseudo-spheroidal coordinate system (ϕ, ξ, μ), where the radial and vertical coordinates are defined as follows:

$$\begin{cases} r^2 = \dfrac{(1-\xi^2)(1-\mu^2)}{1-\omega^2} \\ z = \dfrac{\mu\xi}{\omega}, \end{cases} \tag{2.4}$$

provides solutions for the Poincaré problem. These are expressed in terms of separable modal functions of the form

$$p = P_n^{|k|}(\xi) P_n^{|k|}(\mu) \mathrm{e}^{\mathrm{i}k\phi}, \tag{2.5}$$

where $P_n^{|k|}(\xi)$ and $P_n^{|k|}(\mu)$ are the associated Legendre functions of nth degree and kth order and n and k are integers. Following Greenspan's (1968) notation, the eigenfrequencies can then be evaluated explicitly, and are distinguished by a triple index $\omega_{n,m,k}$, where n and k vary over all integers and m (going from 1 to $n-|k|$ if $n-|k|$ is even, and from 1 to $n-|k|-1$ if $n-|k|$ is odd) corresponds to the mth solution of the transcendental eigenvalue equation:

$$kP_n^{|k|}(\omega) = (1-\omega^2)\frac{\mathrm{d}P_n^{|k|}(\omega)}{\mathrm{d}\omega}. \tag{2.6}$$

For this set of modes, the three components of the velocity field are also explicitly computable (Zhang *et al.* 2001). Experimental evidence of Bryan's modes had to wait 80 years, when Aldridge & Toomre (1969) directly measured inertial resonant eigenfrequencies of a rotating sphere, lately numerically confirmed by Rieutord (1991). Although the experimental results are highly dependent on the measurement method (Zhang *et al.* 2013), they showed excellent agreement with those theoretically predicted solving (2.6). Another experimental confirmation of the existence of inertial modes in precessing spheroidal cavities (and of their propagation along conical surfaces) is found in Noir *et al.* (2001).

2.2. *The WKBJ limit*

In the case of inertial waves in a spherical container, a new WKBJ formalism has been recently developed in astrophysical context in order to solve an approximated version of (2.6) and to investigate the inviscid spectrum and the spatial structure of the associated normal modes (Arras *et al.* 2003; Wu 2005*a*; Ivanov & Papaloizou 2010). This spectrum is well-defined despite the fact that inertial waves have a discrete but everywhere dense spectrum (Lockitch & Friedman 1999).

One example of a spectrum obtained with this methodology is presented in Ivanov & Papaloizou (2010). In order to meet the short wavelength limit, required by WKBJ theory, the asymptotic form of the Legendre functions in the limit of large values of n is used. They then compute the approximate first-order expression for the eigenfrequencies from (2.6):

$$\omega_{n,m,k}^{WKBJ} = \cos\left(\pi\frac{m+1/4-|k|/2}{n+1/2}\right). \tag{2.7}$$

Remarkably, for large n, m and k, this expression explicitly shows the degeneracy of the spectrum in terms of scale redundancy, obtained by replacing $(n, m, k) \rightarrow$

$j(n, m, k)$. Eigenfrequencies obtained in the WKBJ limit have been tested against previous numerical results (Lockitch & Friedman 1999; Dintrans & Ouyed 2001) and have shown surprisingly good agreement even for the so-called 'global modes', whose perturbation involves the whole domain, and for which the WKBJ approach is not expected to constitute, in principle, a meaningful approximation.

In terms of direct comparison with eigenfrequencies computed solving (2.6) and (2.7), we can take, as an example, the least-damped axisymmetric inertial mode in the full sphere, $\omega_{4,1,0} = \sqrt{3/7}$ (Dintrans *et al.* 1999; Rieutord *et al.* 2001). This corresponds, in this WKBJ formalism, to $\omega_{4,1,0}^{WKBJ} = \sin(2\pi/9)$. The difference between the two values is $O(2\,\%)$.

Using this WKBJ limit, solutions for the associated wavefield are computed (Wu 2005*a*; Ivanov & Papaloizou 2010), that can be compared with numerical and analytical results. A noteworthy feature is that the largest pressure perturbations, as well as the steepest spatial gradients for pressure and velocities, are to be found near the surface of the sphere, and in particular at the 'critical latitudes', where the inclination of the rays matches the inclination of the local tangent to the boundary. These locations have turned particularly important in, for example, the tidal dissipation problem (Wu 2005*b*). These hot spots are in general not visible for the low modes computed using Zhang *et al.*'s (2001) explicit formula, but will play a crucial role for ray trajectories, as we shall see in § 3.

2.3. *Three-dimensional ray tracing*

In addition to the analytical approach (§ 2.1), and in parallel to the WKBJ approach introduced in § 2.2, geometrical ray tracing constitutes a third, useful technique for the study of inertial waves in enclosed domains. We briefly review in this section the three-dimensional ray tracing algorithm, while the interested reader is referred to § 2.2 and the appendix of Rabitti & Maas (2013) for the construction of the map that relates a reflected to an incident ray.

In fact, in an appropriately rotated version of (2.2), a plane wave perturbation can be described in two dimensions only, containing the vertical axis (z), aligned with rotation, and one horizontal axis (x), aligned with the propagation direction. Substituting a wave-like solution for pressure $p \propto \mathrm{e}^{\mathrm{i}(kx+mz)}$, the dispersion relation follows:

$$\omega^2 = \sin^2\theta, \tag{2.8}$$

where the wavevector is now expressed in polar coordinates as $\boldsymbol{k} = (k, m) = \kappa(\cos\theta, \sin\theta)$, with θ the angle between the wavevector and the horizontal. Since ω is independent of wavevector magnitude κ (see (2.8)), it follows that for internal waves, group velocity ($\boldsymbol{c}_g = (c_{g,x}, c_{g,z}) = \boldsymbol{\nabla}_{\boldsymbol{k}}\omega$) is perpendicular to phase velocity ($\boldsymbol{c} = (\omega/\kappa^2)\boldsymbol{k}$), and points along a direction having an angle θ with the vertical. In other words, this reveals the interesting fact that internal waves are monoclinic and not monochromatic.

It follows that internal wave group velocity in stably stratified fluids is directed along beams, the internal wave rays, whose inclination with respect to the restoring force is uniquely set by the frequency of the perturbation, and the environmental condition (density stratification and/or rotation) (Görtler 1943; Greenspan 1968), and this inclination is conserved upon reflection at the domain's boundaries.

Now we want to trace the behaviour of a perturbation at definite frequency ω. The perturbation is thus 'launched' at one location, at position $\boldsymbol{x}_0 = (x_0, 0, z_0)$. Note that the x-axis is now defined by the position of the launching point, and not by the propagation direction as for (2.8). It is clear that we can choose $y_0 \equiv 0$ because of axial

symmetry of basin and equations. We shall see in § 6 how this kind of experiment would be practically feasible.

One crucial difference with respect to the usual two-dimensional setting has to be pointed out. When a three-dimensional problem is studied, the launched perturbation is then allowed to travel along characteristic cones, given by the 2π revolution of the classical, two-dimensional St. Andrew's cross, whose aperture 2θ is uniquely set by the perturbation frequency and the stratification/rotation properties via the dispersion relation (2.8).

One single ray will then be uniquely defined by four parameters: ω, which sets the vertical propagation angle θ; $\boldsymbol{x}_0$, which fixes the launching position; the initial horizontal direction ϕ_0 in the xy-plane, measured anticlockwise with respect to the x-axis, which identifies one upward and one downward propagating rays from the others belonging to the same excited internal wave double cone; and $\gamma_0 = \mathrm{sign}(c_{g,z})$, that finally and unequivocally distinguishes either the upward or the downward propagating ray.

In the subsequent ray path computations, we adopt a vertical coordinate stretching:

$$z' = \frac{z}{\lambda} = \frac{z}{\cot\theta} \tag{2.9}$$

in order to fix the ray's inclination to an angle $\theta' = 45^\circ$ with respect to the vertical, for any perturbation frequency. This change of variable implies a strong simplification in the calculations, the only price being the vertical compression or elongation of the spherical domain into an oblate ($\omega < 1/\sqrt{2}$) or prolate ($\omega > 1/\sqrt{2}$) spheroid. To facilitate the reader, all figures in this paper have been subsequently restretched back to the original spherical geometry, without compromising the validity of the results.

The new direction into which the ray (representing the energy propagation direction of an incident wave beam) scatters upon reflection from a sloping boundary is determined as follows (Phillips 1963; Hughes 1964). Since the wave frequency does not change, also the beam's angle with respect to the vertical does not change at reflections from the boundaries: this is equivalent to requiring that the incident and reflected waves obey the same dispersion relation (2.8), while the boundary condition of vanishing normal flow at the reflection point needs to be also always satisfied. The mechanism of horizontal scattering of the ray is sketched in figure 1, and explained in detail in the appendix of Rabitti & Maas (2013). While the wavevector component in the along-slope, tangential direction is unchanged, the wavevector component in the cross-slope direction changes due to a focusing or defocusing reflection, depending on the local bottom slope $s = |\nabla H|$. The new horizontal direction (ϕ_r) of the reflected ray is, in fact, completely determined by the horizontal direction of the incoming wave, ϕ_i and the local bottom gradient itself (see figure 1*c*).

When the transformation in (2.9) is used, conservation laws and geometrical laws (Phillips 1963; Eriksen 1985; Gilbert & Garrett 1989; Manders & Maas 2004; Maas 2005) yield the relation between ϕ_i and ϕ_r:

$$\sin\phi_r = \frac{|s^2 - 1|\sin\phi_i}{2s\cos\phi_i + s^2 + 1}. \tag{2.10}$$

When the reflection takes place where the local bottom slope is smaller than the inclination of the ray ($s < \tan\theta' = 1$), the reflection is called subcritical and it leads to a change in sign of the vertical component of the ray's velocity $\gamma_r = -\gamma_i$. In the opposite scenario ($s > 1$), the reflection is called supercritical and no change in sign is

involved. Critical latitudes (θ_c) connect critical points at which the bottom slope equals the ray slope ($s = 1$), and they lead, in the projection on the horizontal plane, to a specular reflection of the incident ray. A detailed description of the different reflection mechanisms in the different parts of the domain, with special attention to the critical latitudes, is given in the appendix of Rabitti & Maas (2013).

The inertial wave ray path for a given frequency ω and initial launching position and direction ($\boldsymbol{x}_0$, ϕ_0, γ_0) can thus be followed as it bounces through the sphere applying the known reflection laws by computing subsequent reflection points.

2.4. *Ray tracing and wavefield reconstruction*

An advantage of using ray theory in a two-dimensional context is that with simple geometrical arguments, given a perturbation frequency and a container shape, one is able to deduce properties of the corresponding internal wavefield, such as its regularity, the nature of its spectrum and the spatial distribution of the energy in the domain.

In two-dimensional settings, the correspondence between closed trajectories and regular solutions on the one hand, and between attracting trajectories and singular solutions on the other hand, can be exploited also when reconstructing the physical field (velocity, pressure) underlying the system in consideration. In fact, rays carry an invariant quantity, called partial pressure, that can be set on specific intervals (so-called 'fundamental intervals') along the boundary, and pressure can be consequently inferred at any location of a two-dimensional domain by summing the two partial pressures carried by the two rays crossing that location and coming from/going to the fundamental intervals (Maas & Lam 1995). With this perspective, it follows that a two-dimensional ergodic orbit (that touches all points of the domain) corresponds to the trivial, motionless solution, since it carries in all points of the domain the same value of partial pressure, thus leading to a uniform pressure everywhere.

Similar arguments are also used in the case of two-dimensional surface gravity wave and electromagnetic wave systems, where the wavefield is determined in any point of the fluid domain, combining waves following rays crossing that point from any direction. For periodic orbits this is a finite sum, for chaotic orbits a continuous sum over all possible directions (Heller 1984). In the related field of quantum chaos such a sum over chaotic orbits is determined by Gutzwiller's trace formula (Gutzwiller 1990).

When two-dimensional, vertically propagating internal waves in a regular domain are considered, for any given eigenfrequency ω of the system, each trajectory is closed (periodic), regardless of launching position ($\boldsymbol{x}_0$) and direction ($\phi_0 = 0, \pi$, the only two possible directions in two dimensions). It follows that each eigenfrequency presents an infinite number of geometrically closed trajectories. Considering $\omega^2 = \sin^2(2\pi/3)$ in a circular domain, four periodic trajectories (out of the corresponding infinite set) are shown in figure 2. Their shapes depend on the position of the reflection points, so that any point of the domain boundary is touched by one of these closed orbits. Since the partial pressure on each trajectory can be set at will, this infinite ensemble of periodic orbits indicates, as in (2.7), the infinite degeneracy of the eigenspectrum, characteristic of symmetric internal wave problems (Münnich 1996), and allows calculation of the wavefield at each point of the domain. It follows that in sufficiently symmetric two-dimensional domains the value of ω is the only parameter controlling the existence of closed ray trajectories and, consequently, of the regularity of the associated field. We will see in § 3.1 that this ceases to be valid for three-dimensional settings, and other parameters will come into play.

The complete three-dimensional reconstruction of the underlying physical fields, using a three-dimensional analogue of the fundamental intervals (from segments to

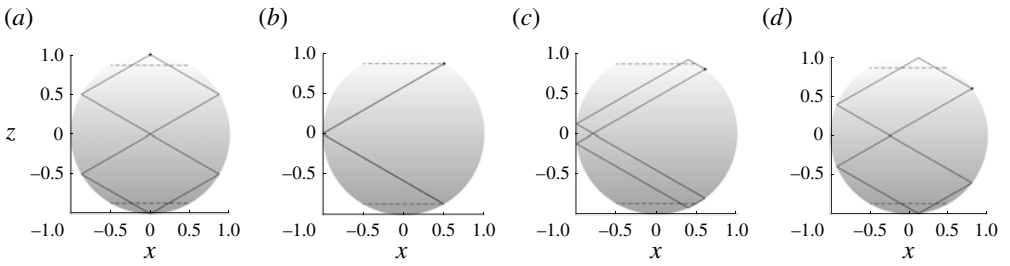

FIGURE 2. Four two-dimensional closed trajectories for $\omega^2 = \sin^2((2\pi)/3)$ in the circle. The orbits differ in launching position x_0 (black dot): (*a*) $x_0 = 0$, (*b*) $x_0 = 0.5$, corresponding to the critical latitudes for this frequency, (*c*) $x_0 = 0.6$ and (*d*) $x_0 = 0.8$. Dashed lines mark the critical latitudes in the two hemispheres. One fundamental interval is $[x, \sqrt{1-x^2}]$, $x \in [0, x_{\theta_c}]$ (Maas & Lam 1995), where x_{θ_c} corresponds to the radial distance from the rotation axis at the critical latitude.

areas?) is far beyond the scope of this work. Thus, in the following, stress will be posed on the qualitative description of the newly observed three-dimensional orbits, while further effort is certainly needed towards a rigorous reconstruction of the corresponding pressure and velocity fields from these geometrically computed trajectories.

3. Results

3.1. *Preliminary comments*

In this section, results from the application of the three-dimensional ray tracing algorithm in the fluid sphere are presented.

Before doing that, it is necessary to point out one fundamental difference between two-dimensional and three-dimensional ray tracing. As seen in § 2.4, for the two-dimensional setting, when an eigenfrequency is excited, any point of the boundary can act as a source for a closed orbit. This leads to the results illustrated in figure 2, where ω is fixed, rays are launched in the meridional plane: $\phi_0 = 0$ or $\phi_0 = \pi$, corresponding to wave energy propagation along the ray path in one sense or the other, and $\boldsymbol{x}_0$ can vary.

By contrast, when the full three-dimensional sphere is considered, ϕ_0 can in principle assume any value in $[0, 2\pi[$, γ_0 can have both signs, and this generality is lost. In practice, of course, couples of ϕ_0 and γ_0 are considered valid only if they generate a ray lying inside the spherical domain, but this results, however, in multiple possible combinations.

In order to generate a geometrically periodic trajectory, frequency ω, position $(\boldsymbol{x}_n)$, horizontal propagation direction (ϕ_n) and vertical propagating direction (γ_n) need to be known in at least one reflection point (n) along the ray path. For convenience, we will generally set such a point as the launching position $(n = 0)$.

From this it is clear that the nature of three-dimensional periodic trajectories is profoundly different from the known two-dimensional periodic orbits. Without knowledge of the whole set of parameters $(\omega, \boldsymbol{x}_0, \phi_0, \gamma_0)$, periodic trajectories are impossible to visualize geometrically. Owing to this strong restriction it was initially believed that three-dimensional periodicity was absent, even in fully symmetric three-dimensional geometries, as hypothesized in Dintrans *et al.* (1999), where, however, only two-dimensional (meridional) ray tracing was contemplated.

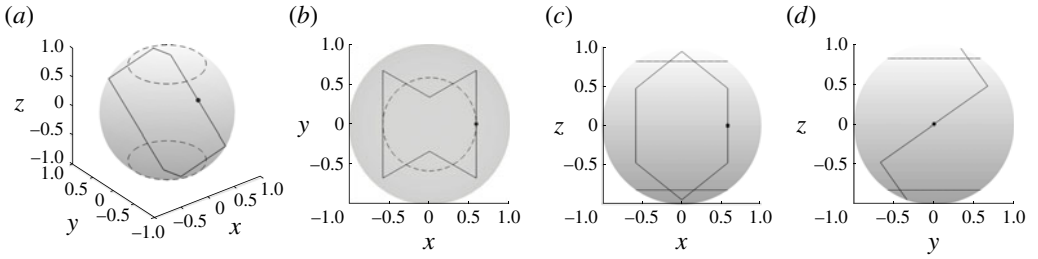

FIGURE 3. Bow-tie periodic trajectory at $\omega^2 = 2/3$: (*a*) three-dimensional view (x, y, z), (*b*) top view (x, y), (*c*) side (x, z) and (*d*) other side (y, z) view. Dashed lines correspond to critical latitudes; black dot corresponds to launching position.

3.2. *Finding one periodic orbit in the sphere*

Given the reflection laws as presented in § 2.3, it is possible, in principle, to estimate valid sets of parameters $(\omega, \boldsymbol{x}_0, \phi_0, \gamma_0)$ representative of simple periodic trajectories in a sphere. In fact, in some simple cases, when the shape of a closed trajectory is known (or guessed), an *ad hoc* system of conditions on launching position $(\boldsymbol{x}_0)$, direction (ϕ_0, γ_0), and frequency of the perturbation (ω) can be solved analytically and all parameters can be determined at one single reflection point.

We started our search with one of the simplest possible trajectories, a 'bow-tie' shaped trajectory (named after its top view appearance, figure 3*b*) and we solved the associated system (see appendix A for details), finding a three-dimensional periodic orbit in a sphere, associated with $\omega^2 = 2/3$ and displayed in figure 3.

Unfortunately, not all geometrically closed trajectories could be solved that easily, since the orbit shape is not known *a priori*, and these periodic orbits do not possess any attractive power, as we expect for a spherical geometry. However, the existence of this single periodic orbit motivated the challenging quest for more.

3.3. *Catalogue of periodic orbits in the sphere*

In figure 4 the frequencies corresponding to periodic orbits observed so far are presented. They are classified according to their appearance and their geometrical properties: given a frequency ω, an initial launching position x_0 and an initial direction ϕ_0, γ_0, we can in fact define the winding number (w) of a trajectory as the total number of times that the trajectory travels around the centre before concluding a full period, defined after R reflections, when $\boldsymbol{x}_R = \boldsymbol{x}_0$, $\phi_R = \phi_0$ and $\gamma_R = \gamma_0$. Whereas some of the frequencies associated with periodic orbits are known algebraically (i.e. those found thanks to the solution of simple algebraic systems as in appendix A or of (2.6)), the majority of the frequencies are known only up to numerical precision. Analogously, periodicity of the orbit has also been tested up to numerical precision, showing, however, its robustness and consistency, even when inspected in the corresponding phase space (see § 3.9).

Different markers in figure 4 correspond to different geometrical features of the orbits. A trajectory is called a 'polygon trajectory' when, in the (x, y) top view it corresponds to a regular polygon (triangle, square, pentagon, hexagon, etc.), see examples in figures 5–7. A trajectory is called a 'star trajectory' when, in top view, it resembles a star, with its typical crisscross pattern, see examples in figures 8, 9 and 22. Both polygon and star trajectories live in what could be called the 'inner

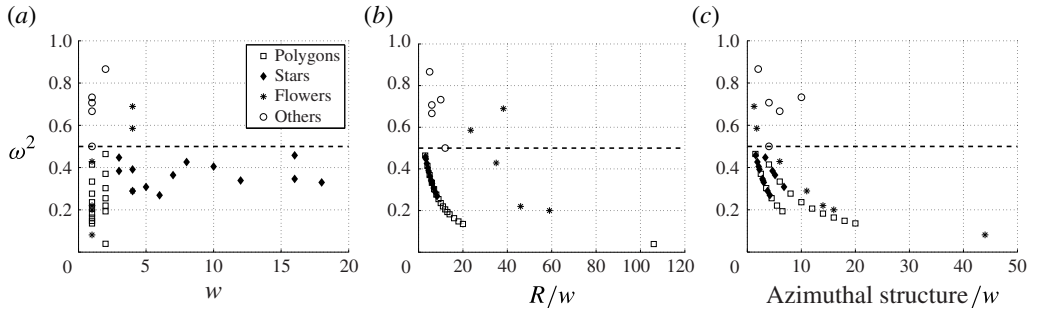

FIGURE 4. Symbols denote squared frequency–azimuthal feature corresponding to observed periodic orbits in the sphere. Different symbols indicate different shapes of the orbits, according to the legend. Names of the categories are explained in the text. In the three subfigures, the same frequencies are classified according to different aspects of their geometrical behaviour. On the x-axis, in (a) we show the winding number, in (b) we show the total number of reflections per period (R) over the winding number and in (c) we show the number of corners (for polygons, stars) or lobes (for flowers and others) over the winding number. The frequencies here presented do not represent the complete spectrum.

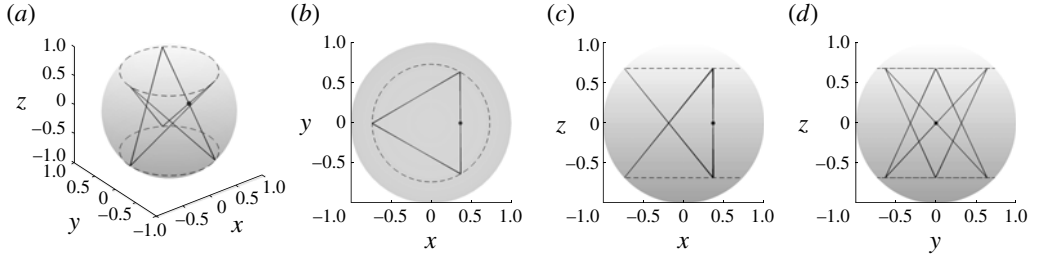

FIGURE 5. Periodic polygon trajectory (triangle) at $\omega^2 = 2\sqrt{3} - 3$, as in figure 3. Winding number is equal to 2.

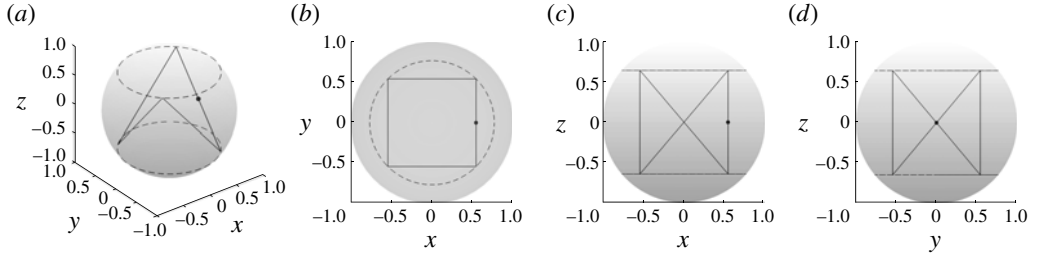

FIGURE 6. Periodic polygon trajectory (square) at $\omega^2 = \sqrt{2} - 1$, as in figure 3. Winding number is equal to 1.

part' of the full sphere, that is inside the cylindrical inset determined by the northern and southern critical circles (indicated by dashed lines in the figures). By contrast, a trajectory is called a 'flower trajectory' when, seen from above, it presents rounded lobes (petals), as in figures 13, 14 and 23. These orbits live only in the 'outer part' of the full sphere, defined as the part of the sphere outside the above-mentioned cylinder.

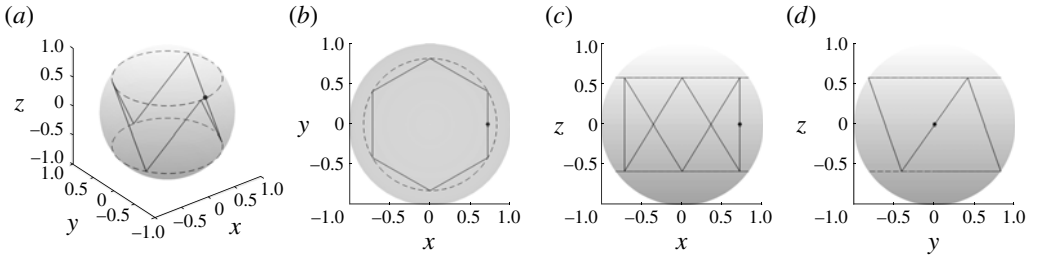

FIGURE 7. Periodic polygon trajectory (hexagon) at $\omega^2 = 1/3$, as as in figure 3. Winding number is equal to 1.

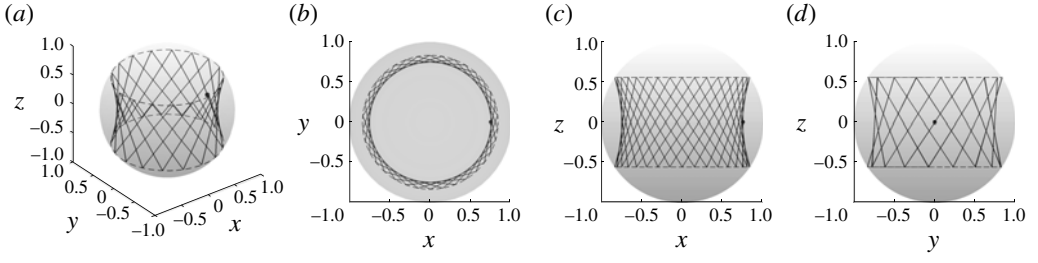

FIGURE 8. Periodic star trajectory at $\omega^2 = 0.3083$, as in figure 3. Winding number is equal to 5.

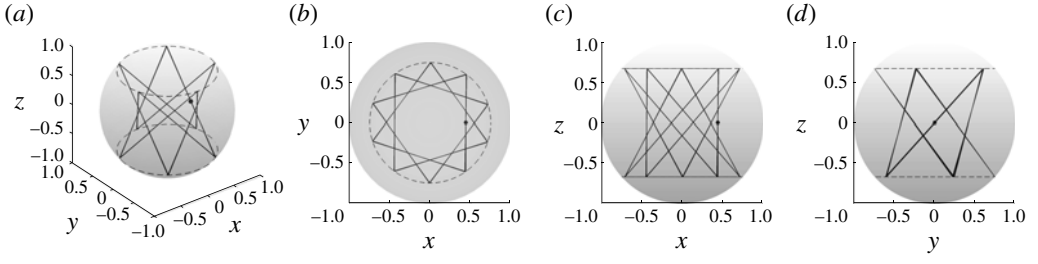

FIGURE 9. Periodic star trajectory at $\omega^2 = 0.4473$, as in figure 3. Winding number is equal to 3.

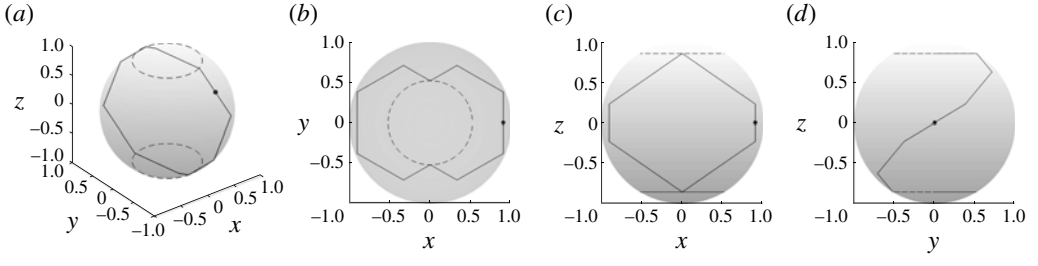

FIGURE 10. Periodic trajectory at $\omega^2 = \sqrt{3} - 1$, as in figure 3. Winding number is equal to 1.

Periodic orbits in the higher-frequency part of figure 4 ($\omega^2 > 1/2$) present less obvious and evocative geometrical properties, and examples are shown in figures 3, 10 and 11.

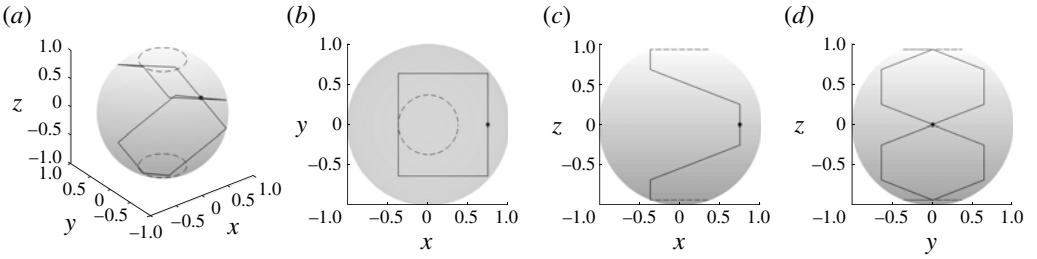

FIGURE 11. Periodic trajectory at $\omega^2 = 0.8660$, as in figure 3. Winding number is equal to 2.

It is worth noting here that as the frequencies depicted in figure 4 are certainly not representative of all of the periodic orbits existing in the sphere, it is also possible that entire other families of trajectory shapes live in the same domain, that have simply not been visualized yet, because, for example, of a counterintuitive three-dimensional behaviour.

In fact, even for simple shapes, as the triangle, the ray behaviour is complicated by the three-dimensionality of the system. Looking from above is indeed not enough to understand one orbit, and we have to move view point, from figure 5(*b*) to a three-dimensional view as in figure 5(*a*) to fully appreciate the trajectory. For many orbits, we observe that a ray needs to wind around the sphere multiple times before completing a period. Comparing figures 5(*a*) and 6(*a*) it is easy to acknowledge the difference between, respectively, an orbit characterized by $w = 1$ (the square) and one characterized by $w = 2$ (the triangle).

In figure 4(*a*) frequencies are plotted against the winding number; in figure 4(*b*) the same frequencies are plotted against the total number of reflections per period (R) over the winding number, while in figure 4(*c*), they are plotted against the number of corners (for polygons, stars) or lobes (for flowers and others) over the winding number. Interestingly, looking at figure 4(*b*,*c*), polygon and star trajectories seem to lie on certain lines, whose definition however remains obscure.

However, according to the geometrical behaviour of the trajectories it is possible to distinguish between two fundamental frequency regimes: (i) $\omega^2 < 1/2$, when, according to (2.9), the domain is compressed to an oblate spheroid; (ii) $\omega^2 > 1/2$, when it is stretched to a prolate spheroid. In figure 4 the frequency $\omega^2 = 1/2$ is marked by a dashed line.

We shall revisit each regime in §§ 3.4 and 3.5. The special case when $\omega^2 = 1/2$, and the domain is thus maintained as a sphere, is presented in § 3.6. One geometrical behaviour is observed both for $\omega^2 < 1/2$ and for $\omega^2 > 1/2$ and is presented in § 3.7, whereas the great majority of the orbits, the non-periodic ones, is discussed in § 3.8. We point out that all periodic orbits found so far in the sphere are 'not isolated' (Berry 1981), in the sense that, if one periodic orbit is given, a continuous family of new periodic orbits can be produced by revolution of the domain. Noticeably, this is true only if this revolution is performed around the stratifying direction (in this case, the z-axis). The whole family is then constituting an ensemble of infinite periodic orbits, filling however only a portion of the domain, and thus profoundly differing from the infinite set existing in two dimensions and presented in § 2.4. Properties of the observed orbits in their corresponding phase space are discussed in § 3.9. We remind that we do not consider here frequencies of the kind $\omega = \sin((p\pi)/q)$, since they have

already been studied extensively in two-dimensional (meridional) settings (Barcilon 1968; Dintrans *et al.* 1999; Rieutord *et al.* 2001).

3.4. *Periodic orbits for* $\omega^2 < 1/2$

Two classes of trajectories are found in the frequency regime $\omega^2 < 1/2$: polygon and star trajectories.

Regarding the polygon trajectories, we observe that polygons with an even number of vertices, are characterized by winding number $w = 1$ (see figures 6 and 7), while polygons with an odd number of vertices have $w = 2$ (see figure 5). Two examples of star trajectories are shown in figures 8 and 9.

Qualitatively, all trajectories in this frequency range present extremely regular spatial patterns, from a triangle up to a 20-sided polygon, and similarly for the star shapes. Moreover, in this regime, it is clear that the critical latitudes play a crucial role in confining all trajectories to the equatorial belt of the cylinder inscribed in the spherical domain, a role that is lost in the orbits in the higher-frequency range (see § 3.5). Exploiting the regularity of the trajectories and the prominent role played by the critical latitudes in this regime, we have been able to deduce some general rules that can be used to evaluate the parameters $(\omega, \boldsymbol{x}_0, \phi_0, \gamma_0)$ needed to find a closed orbit. These rules are listed in appendix B, and constitute the reason why periodic orbits of polygon or star shapes are the most numerous in figure 4. Following these rules it is easy to evaluate, for example, the parameters for the square trajectory (figure 6). If we set as launching point $P_0 = \{x_0, 0, 0\}$ (not on the boundary), as in figure 6(*b*), and $\phi_0 = \pi/2$, then the following conditions for the upper right corner P_1 (in the xy-plane) follow: (i) $x_1 = x_0$; (ii) $x_1^2 + y_1^2 = r_{\theta_c}^2 = 1 - \omega^2$, the point belongs to the circle corresponding to the critical latitude (see appendix B for details); and (iii) $z_1^2 = x_1^2$, the ray moves at $\pi/4$ with respect to the vertical. The system is then easily solved and gives $\omega^2 = \sqrt{2} - 1$.

The other frequency regimes do not present such a regularity in the trajectory patterns, thus no rules have been deduced and consequently less closed trajectories have been visualized.

From a top view, these two orbit categories closely resemble the two types of orbits present in a classical, two-dimensional ellipsoidal billiard (see § 6 of Berry 1981), where the critical latitudes of the sphere act as the boundary of the two-dimensional elliptical domain. The apparently inconsistent fact that we observe the same pattern emerging from a perfectly circular two-dimensional projection (on the x, y-plane) of the sphere is due, first, to the different reflection laws and, second, to the complexity introduced here by the third dimension. More on this kind of comparisons will be discussed in § 3.9.

3.5. *Periodic orbits for* $\omega^2 > 1/2$

In the prolate case, $\omega^2 > 1/2$, the closed trajectories here presented have been evaluated analytically one by one, solving *ad hoc* systems of equations, in order to construct geometrically simple closed trajectories (see an example of these systems in appendix A). Examples of periodic trajectories for this regime are shown in figures 3, 10 and 11.

Due to their irregular patterns, no general rules have been deduced for closed trajectories in this frequency regime, and this is also why orbits in this regime are scarce and scattered (see figure 4). Moreover, in this case, the critical circles do not

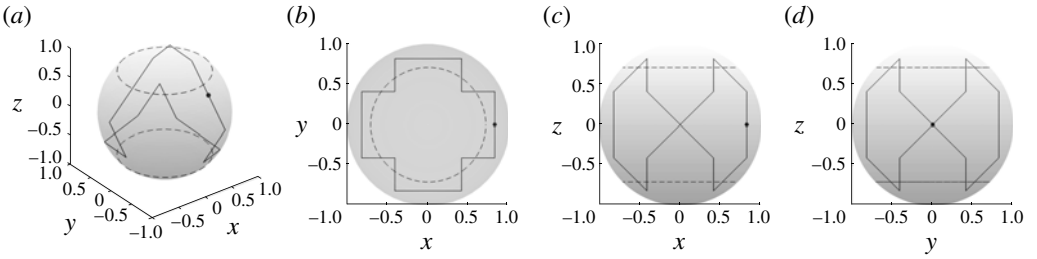

FIGURE 12. Closed trajectory at $\omega^2 = 1/2$, as in figure 3. Winding number is equal to 1.

seem to play such a prominent role in the trajectories, meaning that rays are not confined to the outside or to the inside of the cylindrical inset defined by the critical latitudes (see, for example, figure 3).

In contrast to the general regularity and azimuthal symmetry characterizing trajectories in the oblate regime, closed trajectories in the prolate spheroid show a more asymmetrical behaviour, especially with regards to the reflection locations in the northern and in the southern hemisphere (see figures 3*d*, 10*d* or 11*c*). We shall come back to this aspect at the end of § 6.

3.6. *Periodic orbit for* $\omega^2 = 1/2$

A regular, three-dimensional periodic orbit is found at $\omega^2 = 1/2$, corresponding to the case when rays have a genuine inclination of 45° with respect to the vertical, and the domain is therefore unstretched by (2.9). The trajectory is shown in figure 12. Remarkably, the critical latitudes are not part of this orbit, nor constitute a spatial barrier for the ray, rendering this orbit similar in features to those presented for $\omega^2 > 1/2$ in § 3.5.

Interestingly, the existence of a frequency value that separates two frequency regimes (and, consequently, two different orbit dynamics) resembles the role of the parameter δ in Berry (1981). The latter was used for the parametric definition of the external boundary of the Snellian oval billiard, and also determines two different regimes for periodic orbits in that setting.

3.7. *Periodic orbits for* $\omega^2 \lessgtr 1/2$

Only one family of trajectories is found both when $\omega^2 < 1/2$ and $\omega^2 > 1/2$: the 'flower' trajectory (examples in figures 13 and 14). Even for this type of trajectory, no general laws have been deduced, although in this case, in parallel to the case of $\omega^2 < 1/2$, the critical latitudes are observed to constitute a spatial barrier for the orbit, confining in this case the rays to the 'outer' part of the sphere, and to the equatorial belt.

Remarkably, all frequencies corresponding to flower trajectories, both with winding number $w = 1$ (in the frequency regime $\omega^2 < 1/2$) or $w > 1$ (in the frequency regime $\omega^2 > 1/2$), are also obtained as solutions of an eigenvalue problem of the kind (2.6) with $k = 0$ (axisymmetric modes) and $n \in \mathbb{N}$ (Bryan modes). In figure 13, for example, we are looking at the Bryan mode $\{4, 1, 0\}$, where $\omega^2 = 3/7$, a frequency that is of particular interest because, as seen in § 2.2, it has been identified as the least-damped axisymmetric inertial mode in the full sphere (Dintrans *et al.* 1999; Rieutord *et al.* 2001). This trajectory has winding number equal to 1.

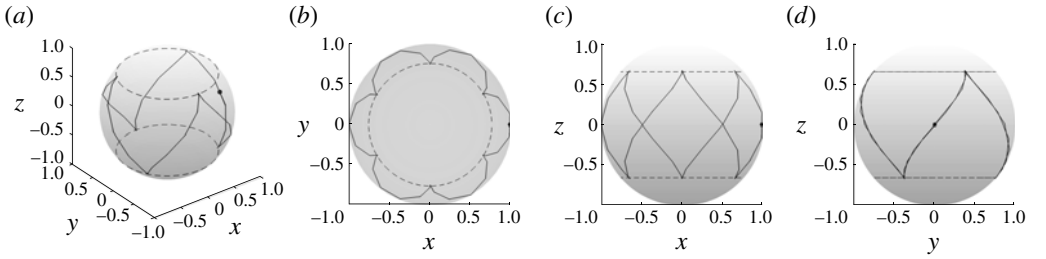

FIGURE 13. Periodic flower trajectory at $\omega^2 = 3/7 \approx 0.4286$, as in figure 3. Winding number is equal to 1.

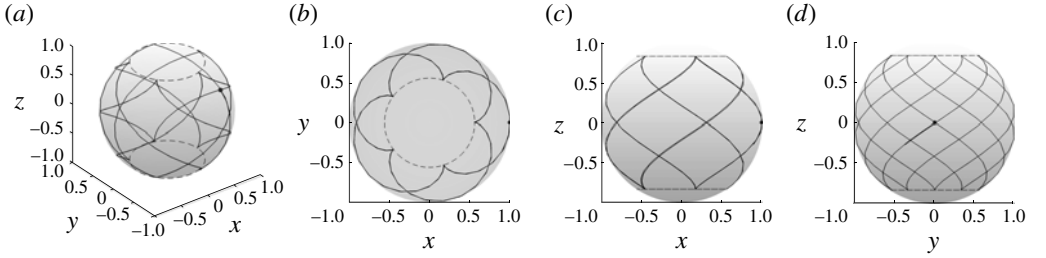

FIGURE 14. Periodic flower trajectory at $\omega^2 = (15 + 2\sqrt{15})/33 \approx 0.6892$, as in figure 3. Winding number is equal to 4.

In figure 14, the Bryan mode $\{6, 1, 0\}$, $\omega^2 = (15 + 2\sqrt{15})/33 \approx 0.6892$ is presented, selected from the possible eigenfrequencies:

$$\omega_{6,1-4,0} = \pm\sqrt{(15 \pm 2\sqrt{15})/33}. \tag{3.1}$$

This trajectory has winding number equal to 4, differently from what it appears looking at figure 14(*b*), that misleads the reader superposing points that belong to different hemispheres (see figure 14*a*).

3.8. *Non-periodic orbits*

So far we have presented only periodic orbits of inertial wave ray trajectories in the full sphere. However, the great majority of combinations of $\omega, \boldsymbol{x}_0, \phi_0, \gamma_0$ leads to non-periodic orbits. In fact, initial conditions for each ray can be taken from two cubes, spanning $\omega \in [0, 1]$, $\boldsymbol{x}_0 \in [0, 1]$ and $\phi_0 \in [0, 2\pi]$ with either $\gamma_0 = 1$ or $\gamma_0 = -1$, and periodic orbits are observed to have a measure zero inside these two cubes. As already mentioned in § 3.4, periodic trajectories so far have been found only because somehow showing regular behaviour, an example of which is explained in appendix B for the lower part of the frequency spectrum, while a random search would not lead to the visualization of any closed trajectory.

Moreover, the periodic orbits found so far seem to act as repellors (and, thus, provide a big contrast to the two-dimensional attractors found in Maas & Lam 1995 and to the three-dimensional attractors found in the spherical shell in Rabitti & Maas 2013), which is why the search has been so challenging. It seems that the sphere exhibits some of the properties characteristic of quantum chaos encountered in elliptic

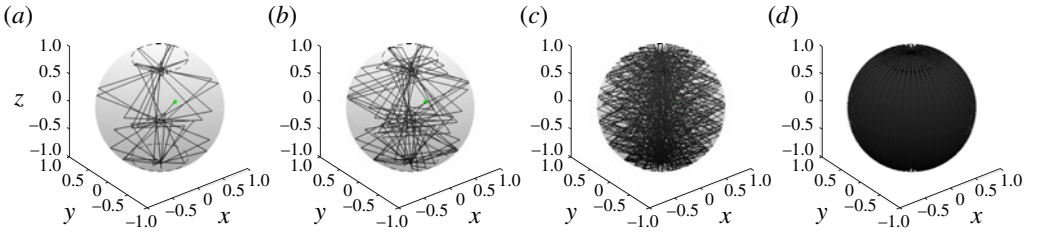

FIGURE 15. Three-dimensional view of invariant trajectory at $\omega^2 = 0.8100$ after (*a*) 50, (*b*) 100, (*c*) 500 and (*d*) 5000 reflections.

systems, in which repelling periodic orbits dominate the response. We shall come back to this aspect in §§ 3.9 and 4.

Interestingly, chaotic and fully ergodic orbits are not found in the sphere. Even if chaos and ergodicity cannot be proved numerically, and a behaviour of this type is suggested by orbits such as that presented in figure 15, when the orbit is inspected in the corresponding parameter space (Berry 1981; Nöckel 1997) it becomes clear that a certain regularity persists, preventing the occurrence of chaotic areas (see § 3.9). With ergodic orbits we mean orbits that fill the sphere homogeneously and, after an infinite number of reflections, touch each point of the domain an infinite amount of times (approaching it from all possible directions on the cone through that point). It follows that ergodic trajectories, such as those present in the case of two-dimensional internal wave rays in the circle, are domain filling, and this is not true for orbits such as that in figure 15 nor for others.

The non-periodic orbits observed in the sphere are, on the other hand, of the so-called 'invariant' type (see § 3.9). Invariant orbits are trajectories that, even if not periodic, are confined to a portion of the domain only, which is usually the equatorial belt (defined between the two critical latitudes), and are continuously repeating themselves and circulating around the domain. An example of these trajectories is given in figure 16. In this case the rays, given an infinite amount of reflections, will densely touch only a subset of points of the full domain. Given a periodic orbit, invariant orbits are easily found by slightly perturbing the frequency, launching point or initial direction. It follows that, for frequencies corresponding to a periodic orbit (as in figure 13), an associated invariant orbit (figure 16) can be obtained by small alteration of x_0 and it fills the same surface that rays would fill in case of axisymmetric forcing at that frequency. This surface corresponds in fact to the subset of boundary points touched by simultaneous excitation (azimuthally symmetric) of the whole ensemble of non-isolated periodic orbits for that specific frequency (see § 6 for application to experimental results).

3.9. *Phase space mapping of the orbits*

So far we have been looking at ray trajectories in real space, however, an alternative representation in the corresponding phase space is also possible, instructive and already used for studying two-dimensional ray dynamics of different nature in closed cavities (Berry 1981, 1987; Nöckel 1997).

In fact, successive reflections can be captured not only by direct ray tracing, as in the previous sections, but also by monitoring the polar angle (χ) at subsequent reflection points as measured from the domain's centre. Combining this polar angle χ

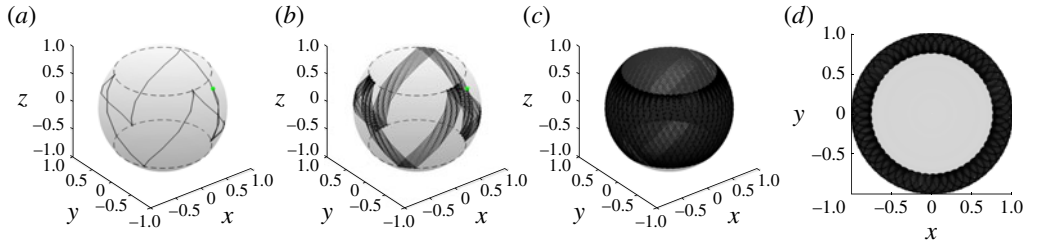

FIGURE 16. Three-dimensional view of invariant trajectory at $\omega^2 = 3/7$ after (*a*) 50, (*b*) 500, (*c*) 5000 reflections and (*d*) top view after 5000 reflections. This figure is obtained using the same parameters as figure 13, but slightly changing the launching position x_0.

at the reflection point with the angle of incidence of the ray relative to the local x-axis (ϕ_i, see figure 1*c*) presents a phase space, in which ray dynamics can be conveniently studied (Nöckel *et al.* 1996).

In this work, even if tracing three-dimensional trajectories, only a two-dimensional projection of the orbit, on the x, y-plane, has been considered, the so-called Poincaré surface of section (SOS, Nöckel 1997). This is motivated by the fact that the third parameter defining each reflection, the inclination with respect to the vertical, is here fixed by the inertial wave dispersion relationship (2.8). The neglect of the three-dimensional representation of the reflection position certainly constitutes a limit to the understanding of these orbits' behaviour, however, we shall present in the following the application of classic SOS to the three-dimensional inertial wave ray trajectories presented in the previous sections, while a definition of a new, three-dimensional phase space, perhaps more appropriate, is left for future work.

In classical mechanics, in phase space (SOS), a periodic orbit appears as a set of isolated points. This is true for two-dimensional as well as for three-dimensional periodic trajectories of internal wave rays. Examples of this phase space in the sphere are shown in figure 17(*a*) for the oblate case (corresponding to the real space trajectory in figure 7) and in figure 17(*b*) for the prolate case (corresponding to the real space trajectory in figure 12); remarkably, all three-dimensional periodic orbits found in the sphere are unstable, and thus referred to as repellors (as opposed to attractors). This means that a small perturbation to the initial conditions is sufficient to infinitely deviate the orbit from the periodic path. As seen at the end of § 3.8, this behaviour is characterizing the majority of the inertial wave orbits in the sphere. Examples of this behaviour are shown in figures 18 and 19, but similar plots (not shown) would be also representative of orbits such as those displayed in figures 15 and 16. This kind of trajectory is characterized, in the corresponding phase space, by the existence of a structure (although highly non-trivial) to which the orbit is confined, and which is therefore called 'invariant'. If looking at SOS of two-dimensional surface gravity wave rays in the circle, these structures are simple straight lines (see figure 3*d* in Berry 1981): in the sphere the regularity of the two-dimensional circular case is probably destroyed by the presence of three-dimensional subsequent (and compensating) focusing and defocusing reflections in a three-dimensional domain, leading to the high level of complexity in figures 18(*b*) and19(*b*).

It is possible, however, to obtain simpler structures. The trajectory in figure 20(*a*) is obtained from the real space orbit in figure 12, when the launching position is moved to the critical latitude. It shows a relatively simple representation in the phase space (figure 20*b*), although its real space azimuthal symmetry properties (figure 20*a*) appear

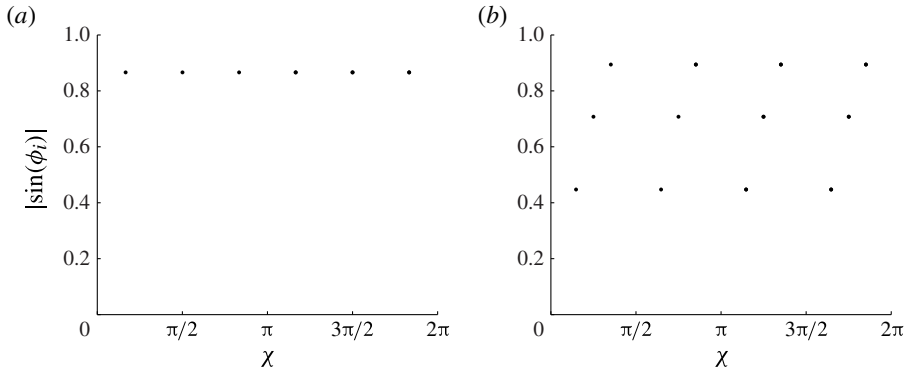

FIGURE 17. (*a*) Poincaré SOS for the polygonal periodic orbits in figure 7. (*b*) SOS for the high-frequency periodic orbits in figure 12. Here χ corresponds to the polar angle pointing at subsequent reflection positions as measured from the domain's centre. Here ϕ_i corresponds to the local angle of incidence of the ray as measured from the local x-axis (see figure 1*c*).

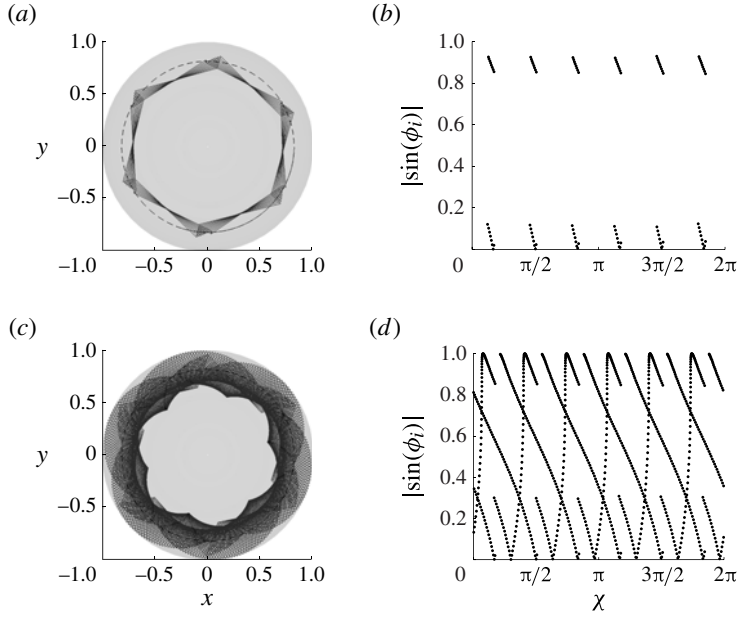

FIGURE 18. (*a*) Top view of invariant trajectory (100 reflections) obtained from the trajectory in figure 7 after perturbing the horizontal launching direction by 0.5 %. (*b*) SOS for the trajectory in (*a*). (*c*) Same as (*a*), after 1000 reflections. (*d*) SOS for the trajectory in (*c*).

to be exceptional when compared with the most common structures, similar to those in figures 18(*a*) and 19(*a*).

Remarkably, this kind of pattern in phase space resembles that characterizing two-dimensional ergodic internal wave orbits, propagating obliquely in the vertical plane in a circle, as shown in figure 21(*b*). However, even if phase space structures

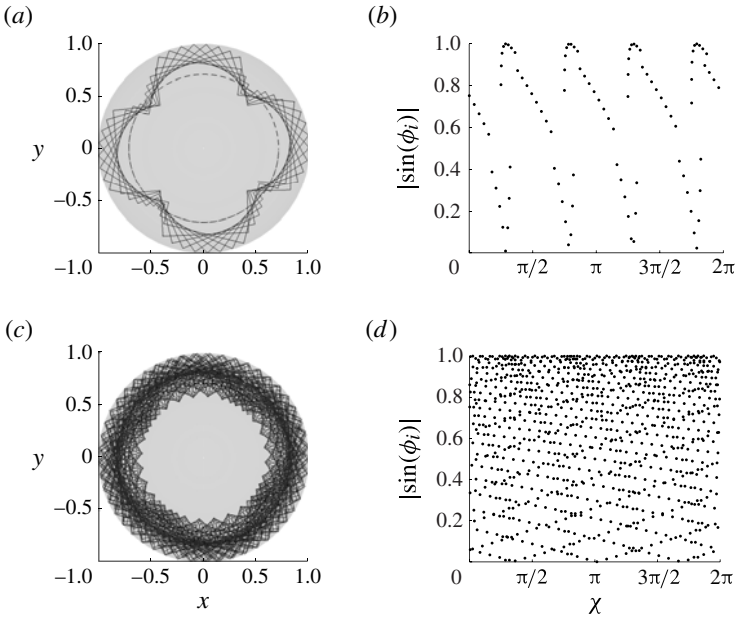

FIGURE 19. (*a*) Top view of invariant trajectory (100 reflections) obtained from the trajectory in figure 12 after perturbing the launching position by 0.5 %. (*b*) SOS for the trajectory in (*a*). (*c*) Same as (*a*), after 1000 reflections. (*d*) SOS for the trajectory in (*c*).

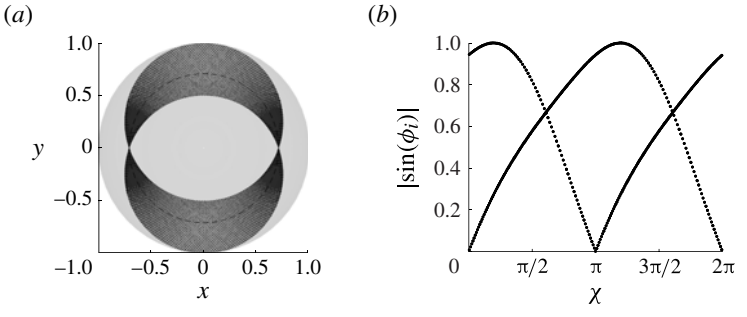

FIGURE 20. (*a*) Top view of invariant trajectory (100 reflections) obtained from the trajectory in figure 12 after setting the launching position at the critical latitude. (*b*) SOS for the trajectory in (*a*).

are similar in the two cases, in the real space three-dimensional invariant orbits (figure 20*a*) profoundly differ from two-dimensional ergodic orbits (figure 21*a*). In particular, the latter are by definition domain filling, while invariant trajectories are clearly limited to a portion of the three-dimensional domain only. This hybrid aspect of the trajectories would probably become clear once studied in an *ad hoc* defined phase space, taking into consideration the full three-dimensional problem.

The third possible type of orbit, the chaotic orbit, would occupy an area in the phase space. Chaotic trajectories are present in two-dimensional elliptical systems in non-regular domains, such as the stadium (Berry 1981), and are likely to be found in three-dimensional hyperbolic systems in symmetry breaking domains as well. On the other

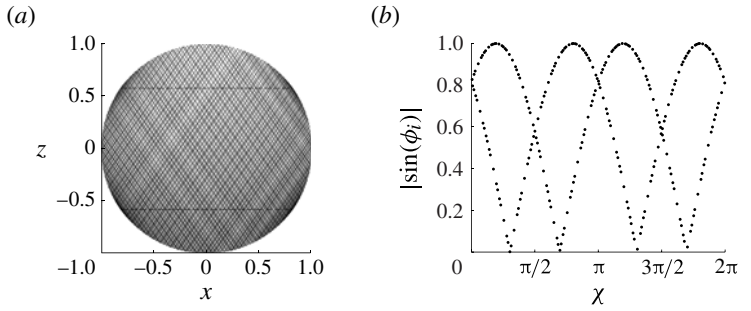

FIGURE 21. (*a*) Ergodic trajectory (250 reflections) in the circle corresponding to the frequency $\omega = \sqrt{1/3}$ (not an eigenvalue). (*b*) SOS for the trajectory in (*a*), here the angle χ refers to the polar angle in the x, z-plane, and ϕ_i to the local angle of incidence relative to the outward radial direction at the point of reflection.

hand, as expected from the overall regularity of the system in analysis, no genuinely chaotic orbit is observed in the case of three-dimensional inertial waves in the full sphere.

4. Discussion

In this work, we have established the existence of three-dimensional periodic orbits for internal wave rays in the full sphere. However, several questions remain on the nature of these orbits, of the associated frequencies and of the underlying wavefield.

In the last few decades, two-dimensional (meridional) ray tracing has been used to investigate the inviscid limit case of inertial waves in the sphere and its known analytical solutions (Dintrans *et al.* 1999; Rieutord *et al.* 2001). In this setting the association between periodic orbits and eigenfrequencies has not been retrieved, for reasons that we now understand. After all, looking at ray tracing only on a meridional plane constitutes a strong limitation if one is interested in the behaviour of inertial modes of the full three-dimensional sphere. In fact, in a spherical domain, if a perturbation is excited within a meridional plane, even when three-dimensional effects are included, it will never escape its original plane. Conversely, if a perturbation is initiated outside a meridional plane, its spatial structure will never collapse onto a meridional plane. But note that this behaviour is strictly representative of that in a regular domain as the sphere, and it is not valid, for example, in a spherical shell, where the interaction of the ray trajectory with the outer and inner sphere gives rise to meridional attracting planes (Rabitti & Maas 2013).

Among all possible zonally propagating waves, existing also in the three-dimensional fluid shell (Rabitti & Maas 2013) and in the parabolic channel (Drijfhout & Maas 2007), the presence of periodic trajectories in the full sphere is suggestive of the resonant character of inertial modes in a regular domain, where the term ‘resonance’ has here not been used in terms of amplitude of the response (see Zhang *et al.* (2013) for a detailed, multi-approach analysis on this subject), but in terms of trajectory coherency.

However, a direct correspondence between closed orbits and classical Bryan’s modes is hardly retrieved (so far, only for the flower trajectories, described in § 3.7). Moreover, the spatial structure of the orbits has been also suggestive of the existence of a relation between the azimuthal wavenumber (when known) and one of the

orbit features (winding number, number of reflections, lobes or corners). Even this correspondence has not yet been retrieved.

One other, perhaps unexpected, aspect of these three-dimensional periodic orbits is encountered if one is interested in the reconstruction of the underlying physical wavefield using the ray's structure. In fact, the observed winding numbers of many trajectories present values larger than one, which is on the one hand puzzling, but on the other hand suggestive of the possibility of adopting non-integer (azimuthal) wavenumbers. We speculate that a pressure function of the separable form (2.5) with rational wavenumbers n and k would also constitute a set of valid solutions for inertial waves in a full sphere, provided that boundary conditions are satisfied (no energy flux through the boundaries, and finiteness in the whole domain, rotation axis and equatorial plane included).

Three-dimensional ray orbits could thus be not only possibly representative of non-separable, zonally propagating solutions, but also of eigenmodes different from those classically obtained from (2.6) using integer degree and order, whose completeness is so far unknown. This would explain the difficulty in relating the periodic orbit with the classic eigenfrequencies of the system.

Furthermore, it is worth noting that in the two-dimensional fluid dynamics case, spatially coherent internal wave beams and trajectories become evident only as a result of the superposition of several modes associated with a single frequency. Owing to the lack of correspondence between rays and eigenfrequencies, and of the complexity of the inversion of (2.6), a rigorous test in this direction could not been performed.

Matching of rays and modes, as also previously pointed out in § 2.2, is also usually expected only in the case of short wavelength limit, and not in the case of large-scale modes. For the higher modes, in fact, the scales of the underlying waves is much smaller than the basin size. Since inertial waves of given frequency have no definite scale, short waves have here to be intended not as, for example, in the quantum chaos case, modes within a certain frequency range, but as modes characterized by large n and k indices (including those of the Legendre functions having non-integer indices n and k), for which it is possible to make good use of asymptotic expansions of the associated Legendre functions. Again, the lack of understanding of the relation between indices n and k and spatial trajectories prohibits to restrict the comparison to high-index Legendre modes.

Interestingly, repelling and unstable periodic orbits such as those observed in this study, profoundly differ both from the plane-filling ensemble of periodic orbits characterizing regular, hyperbolic systems, as described in § 2.4 (see figure 2), and from the classical annulus-filling non-isolated periodic orbits in the circular billiard (elliptic system).

In fact, even if the closed orbits in the sphere are non-isolated under rotation around the z-axis, they remain isolated in a three-dimensional sense, because of the strong interdependency between the parameters $(\omega, \boldsymbol{x}_0, \phi_0, \gamma_0)$.

In this sense, they resemble more the isolated, unstable ray trajectories found in elliptic, classically chaotic systems, such as those describing surface waves in a stadium (Berry 1981, 1987; Kudrolli *et al.* 2001). If we may continue the analogy, it follows that, even if in three dimensions we have no one-to-one correspondence between classic orbits and 'quantum' levels of the system (eigenfrequencies), we can still use the behaviour of the rays as an ingredient for deriving general information on the spectrum and on the regularity properties of a system. This would also help in explaining why only few periodic orbits found their counterpart in terms of Bryan's (1889) modes. Moreover, when inspected in the corresponding phase

space, three-dimensional invariant orbits show a similar behaviour to those of two-dimensional ergodic orbits, although without the crucial characteristics of being domain filling. This combination of different behaviours could be the result of tracing trajectories in a highly anisotropic three-dimensional space, whose anisotropy is set by the presence of the rotation axis (aligned in this case with the vertical). Focusing and defocusing in the vertical direction coexist then with spreading and scarring in the horizontal plane (perpendicular to the stratification/rotation), also because focusing reflections in the vertical plane lead to a change in cross-slope momentum, while not affecting the momentum in the along-slope, tangential direction.

In addition, we have seen from (2.2) that for general (non-symmetric) three-dimensional domain shapes, the system acquires a hybrid character, in between hyperbolic and elliptic problems. Consequently, it may well show asymptotically both periodic attracting orbits, as in the spherical shell (Rabitti & Maas 2013), as well as periodic repelling orbits, as the ones here observed in the sphere, characteristic respectively of singular and regular wavefields. It is also worth noting that such repelling periodic orbits are living in the spherical shell too, provided that rays do not interact with the inner boundary, and that thus attractors, periodic and invariant modes could in principle coexist in the same three-dimensional domain: in fact Maas (2005), Drijfhout & Maas (2007) and Rabitti & Maas (2013) have already shown that attractors and invariant modes (there also called 'edge' or 'whispering gallery' modes), can indeed occur simultaneously in a stratified paraboloid, channel and spherical shell (all symmetry-breaking geometries). In terms of energy content, however, attracting orbits will always prevail over periodic orbits in symmetry breaking geometries, because of the formers' focusing power.

Despite the possible presence of all these different orbits, we are still far from formalizing a field reconstruction on the basis of ray trajectories only. In fact, it is clear that even if an annulus-filling ensemble of periodic orbits exists at a specified ω, this does not constitute the three-dimensional counterpart of the domain-filling infinite ensemble of periodic trajectories that occurs in two dimensions in regular domains for each eigenfrequency (see § 2.4 and figure 2). The infinite three-dimensional periodic orbits are all identical, and summed up they do not cover the whole basin. This implies that evaluating the associated field in the whole domain from rays only remains a non-trivial (if not impossible) challenge.

However, we did find an example of one frequency (although numerical) presenting two differently shaped closed trajectories (figures 22 and 23). It is therefore possible, in principle, that an infinite set of differently shaped periodic orbits exists for each eigenfrequency, mirroring a degeneracy of the associated spectrum. Only if this is true it would be possible to reconstruct the underlying wavefield using a two-dimensional generalization of the one-dimensional fundamental intervals arising in the two-dimensional problems (Maas & Lam 1995).

It has to be clear, in fact, that our limited understanding on how to determine valid parameters ω, $\boldsymbol{x}_0$, ϕ_0 and γ_0, necessary to visualize the ray pattern, restricts our ability to geometrically check and visualize periodicity, but it does not reduce the number of physically valid eigenvalues of the system and, with this, the number and degeneracy of the modes in the system.

5. Summary

Understanding the behaviour of internal waves in fully enclosed domains constitutes one of the big challenges in fluid dynamics, especially because of the numerous

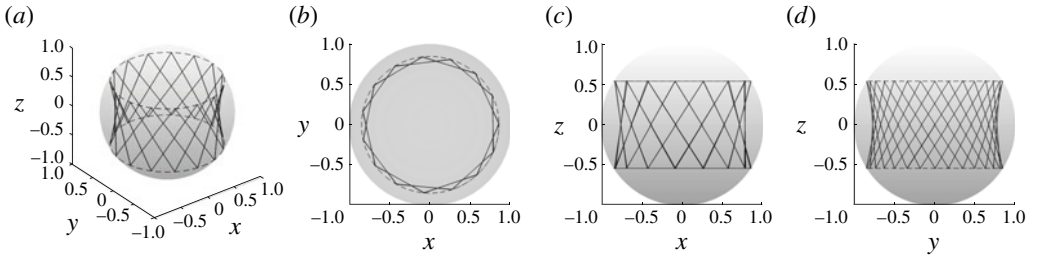

FIGURE 22. Periodic star trajectory at $\omega^2 = 0.2890$, as in figure 3. Winding number is equal to 4.

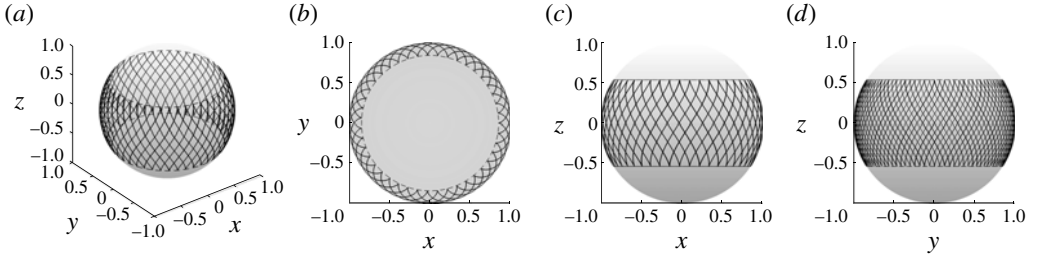

FIGURE 23. Periodic flower trajectory at $\omega^2 = 0.2890$, as as in figure 3. Winding number is equal to 4.

possible applications both in astrophysical and geophysical fluid dynamics. Since analytical solutions for internal waves in arbitrarily shaped domains are not available, numerical approaches or geometrical ray tracing techniques have been widely used in order to infer properties of the underlying wavefield and energy distribution in the container. Ray tracing, commonly used in two-dimensional settings, has recently been extended as a three-dimensional tool, in the direction of a more realistic representation of the corresponding wavefield and of the source of perturbation. However, the significance of three-dimensional internal wave rays has not been completely understood.

In this work, a three-dimensional algorithm of ray tracing has been applied for the first time to the full homogeneous rotating sphere, in order to investigate the nature of three-dimensional inertial wave ray orbits. The sphere in fact is one of the few domains where analytical solutions are known for the linear, inviscid case, and where WKBJ theory has also been commonly applied.

Three-dimensional periodic orbits have been then observed in the sphere. Moreover, two main frequency regimes can be distinguished, according to the different behaviour of the orbits: $\omega^2 < 1/2$ and $\omega^2 > 1/2$.

In the low-frequency regime, three 'families' of periodic orbits are found: polygon, star and flower trajectories, classified because of their appearance in top view. In this regime, the critical circles define an inscribed cylinder that acts as a physical barrier for the orbits, confining the rays to the equatorial belt. This crucial role played in the ray dynamics by the critical latitudes finds its counterpart in the model proposed by Wu (2005*a*), where the critical circles are named 'singularity belts' and right so.

In the high-frequency regime, no regular pattern but of flower type is observed. However, periodic orbits are still present, even if critical circles do not play such a prominent role.

Difficulties in relating the observed periodic trajectories to the simplest eigenfrequencies computed using (2.6) (the Bryan modes) could be due to several reasons, discussed in § 4. Perhaps the most intriguing one is the fact that when a three-dimensional ray tracing algorithm is used, the absence of any assumption on separability of the solutions could unveil the structure of intrinsically three-dimensional modes in the sphere, which remained hidden so far because of the particular form of solutions (2.5), and because of the requirement for the n and k indices to be integer. This perspective certainly requires further investigation.

We are led to think that the periodic orbits observed so far have been limited by our poor understanding of the geometrical properties of these trajectories, and by the human tendency to prefer regular and repetitive patterns such as, indeed, polygons, stars and flower shapes. We also know that the inertial wave spectrum in the sphere is dense (Bryan 1889), therefore a complete catalogue of existing periodic orbits would be of no practical use. In this work only the first proof of the existence of such trajectories is given: further investigations would contribute to a more general perspective on the geometrical features of these trajectories, and to a complete understanding of plots such as those in figure 4 and of the emerging patterns.

Nevertheless, enough and differently shaped closed patterns have been found to deduce some general properties on the periodicity of the orbits and the observation of other trajectories would not change the overall picture of the system. The existence, in fact, of inertial wave, periodic orbits in a regular three-dimensional container such as the sphere allows to extend the usual two-dimensional correspondence between modes and periodic ray trajectories, previously discarded (Dintrans *et al.* 1999), to a three-dimensional setting.

Moreover, the presence of repelling periodic orbits, such as those observed here, and of invariant orbits presenting ergodic aspects, points out the interesting fact that the three-dimensional hyperbolic problem of inertial waves in the homogeneous full sphere presents, in terms of quantum chaology (Berry 1987), some properties typical of elliptic systems. The three-dimensional orbits found so far in the sphere seem to be only of the periodic and of the invariant kind. However, the existence of two different orbit regimes (as in the oval billiard Berry 1981), and of isolated orbits (isolated with respect to rotation around an axis different from the z-axis), are suggestive of a more heterogeneous dynamics. A three-dimensional phase space study will possibly provide further insight in the hybrid nature of these trajectories.

6. Final remarks

We are conscious that geometrical patterns constitute a widely general and fascinating feature of several fluid dynamical systems, including geophysical (Lewis & Hawkins 1982) and astrophysical (Godfrey 1988) contexts. It is therefore worth pointing at the immediate association that arises between the closed hexagonal trajectory in figure 7 (corresponding to an exact frequency $\omega^2 = 1/3$), and the famous hexagonal vortex observed over Saturn's North Pole (Godfrey 1988). Experimental results in a differentially rotating spherical gap (Hollerbach *et al.* 2004), as well as in cylindrical systems (Barbosa Aguiar *et al.* 2010), have shown that polygonal patterns may arise from destabilization of a zonal jet, in the case of meandering of the Stewartson layers that form tangent to the inner boundary, a situation that substantially differs from the configuration object of the present study. To the best of the authors' knowledge, no polygonal pattern has been experimentally observed in a full sphere so far. However, this evidence does not tell much about the possible

existence of resonant periodic orbits in the full sphere for axisymmetric forcing mechanisms such as, for example, libration. In this context, in fact, a single periodic orbit as the ones presented in this study cannot be visualized, since it implies not only a point source of the disturbance, namely, a single launching position $\boldsymbol{x}_0$, but also the selection of a single ray (identified by ϕ_0 and γ_0) within the excited double cone. In practice, this would need an oscillating source, setting the frequency of the radiating perturbation. The selection of a single ray (in two dimensions), or at least of a portion of one of the two cones (in three dimensions), could be then achieved putting the forcing oscillator in one basin (basin 1) that is different from the container in analysis (basin 2), and orienting an aperture between the two basins such that only one single beam, or a portion of one of the cones, is able to propagate from basin 1 to basin 2. In the case of axisymmetric forcing (given by an azimuthal revolution of the launching position), rays will on the other hand occupy a surface, given by the azimuthal revolution of the corresponding periodic trajectory, resembling the corresponding invariant orbits, see figure 16. In this regard, the prominent role played by the critical latitudes in the ray trajectories is in agreement not only with the three-dimensional numerical simulations such as those in Wu (2005*a*), but also with some laboratory experiments in rotating sphere and shell, such as those by Noir *et al.* (2001), Le Bars, Le Dizès & Le Gal (2007) and Koch *et al.* (2013).

Another possible association between previous findings and the newly observed periodic trajectories arises when we look at their symmetry properties. As we have already noticed at the end of §§ 3.4 and 3.5, the geometrical patterns of periodic trajectories of the rays show a strong difference in the two frequency regimes. The low-frequency case ($\omega^2 < 1/2$) shows a strong regularity in the azimuthal and in the vertical direction, while this is not true for the high-frequency case ($\omega^2 > 1/2$). We recall that when we use the variable transformation (2.9), and we do not restretch back our domain, this results in a deformation of the spherical domain into an oblate or a prolate spheroid respectively, according to the frequency explored, while the ray inclination is fixed to 45° with respect to the vertical. This observation recalls some old, and so far not completely explained, experimental results from the end of the 19th century (Lord Kelvin 1877, 1880*a*), when Lord Kelvin and assistants performed a series of experiments to investigate gyroscopic properties of respectively a rotating oblate and prolate spheroidal domain filled with liquid. While the oblate container behaved not noticeably different from the ordinary solid gyrostat, the prolate spheroid presented a 'truly wonderful contrast' as its failure as a gyrostat resulted in the prolate container stopping turning only after a few seconds after its release.

A possible interpretation of the different response between the two geometrical settings comes from the different symmetry properties and ray distributions observed in the three-dimensional periodic orbits found in this study. It is not obvious whether, in general, analysing a frequency in differently shaped containers (Kelvin's approach) or, instead, fixing the inclination of the rays and consequently deforming the container (ray tracing approach) would lead to the same physical system or not, but, if we consider as key parameters only the relative inclinations between (i) the restoring force, in this case rotation, and (ii) the ray trajectory and (iii) the local tangent to the boundary at the reflection point, the two approaches appear at a first view to be completely equivalent. If this is the case, a non-axisymmetric forcing at the surface of the prolate (oblate) ellipsoid would result in a non-axisymmetric (axisymmetric) response of the domain, with (without) consequent triggering of instabilities and possibly of a net torque on the container. Further experimental investigations would certainly provide new light on these historic findings.

Discussing robustness of three-dimensional inertial wave ray tracing in the case of a homogeneous, rotating fluid-filled sphere may seem far from any possible application of practical use, however, inertial waves in the sphere constitute a paradigmatic case for the more general case of internal waves in arbitrarily shaped, fully enclosed domains. Extending our general understanding on wave ray dynamics can thus be crucial towards more realistic, three-dimensional, internal wavefield reconstructions and regularity (or, more commonly, singularity) analysis, as called for by many geophysical and astrophysical challenges.

Acknowledgements

A.R. is supported by a grant from the Dutch National Science Foundation NWO. The authors gratefully acknowledge U. Harlander for the numerous and helpful comments on this work. Thanks are also due to the editor and to the three anonymous referees for their constructive suggestions that largely improved the lucidity of the final form of this manuscript.

Appendix A. Geometric derivation of a closed trajectory: the bow-tie case

According to the reflection laws described in § 2.3, one of the simplest periodic trajectories we can think of is depicted in figure 3. In order to derive its parameters, it is worth remembering that the horizontal refraction law, (2.10), is valid only if angles are defined in the local reference framework of reflection, as shown in figure 1(*c*) for a general case, and in figure 24 for this specific trajectory. The latter is easily prescribed, the local positive x-axis corresponding to the line of local maximum bottom slope, pointing outwards. In figure 24 the different local reference frameworks are referred to as (x, y), relative to the point P_0, (x', y'), relative to the point P_1 and (x'', y''), relative to the point P_2 and they are depicted as grey dashed lines. Moreover, we recall that in the algorithm used, in order to have rays that always move with an inclination of 45° with respect to the vertical, the surface of the sphere is deformed according to (2.9), depending on the perturbation frequency ω, and described therefore by

$$x^2 + y^2 + \lambda^2 z^2 = 1 \tag{A 1}$$

where λ is defined in (2.3). It is now possible to cast the problem in a system of equations, in order to evaluate analytically which combination of ω, x_0, ϕ_0 and γ_0 reproduces this trajectory. The orbit in figure 24 has been constructed as follows: we prescribe a launching point, $P_0 = \{x_0, 0, 0\}$, that lies on the equatorial plane, an initial launching direction $\phi_0 = \pi/2$ and a negative sign of the initial vertical component of the group velocity ($\gamma_0 = -1$). In $P_1 = \{x_1, y_1, z_1\}$ a supercritical reflection takes place: the vertical component of the group velocity does not change its direction, $\gamma_1 = \gamma_0 = -1$, and the ray is refracted inwards, towards the central region of the sphere. By contrast, in $P_2 = \{x_2, y_2, z_2\}$, a subcritical reflection takes place, vertical velocity reverses its sign, $\gamma_2 = -\gamma_1 = 1$, and a defocusing reflection sends the trajectory back up, towards the outer part of the prolate spheroid.

For symmetry reasons, we can restrict the study to the first quadrant of the x, y-plane, setting the condition that a reflection occurs in P_2 that is perfectly symmetric with respect to the x''-axis (coinciding with the y-axis): the ray's path would therefore reproduce in the second quadrant (and in the northern hemisphere) the mirrored pattern of the first one, and so on.

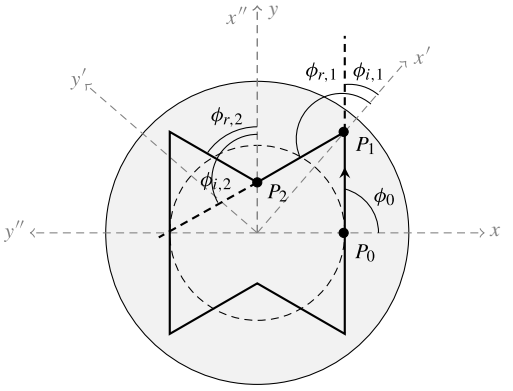

FIGURE 24. Top view projection of bow tie orbit (solid) for $\omega^2 = 2/3$, obtained by three-dimensional ray tracing (as figure 3*b*). Inside (outside) the dashed circle rays reflect subcritically (supercritically) from the bounding sphere. Launching point is at P_0 (on the equatorial plane), initial ray vertical direction is downward, while horizontal direction is ϕ_0. The ray is thus travelling in the direction indicated by the black arrow. The two reflection points in the first quadrant are P_1 (in the supercritical area, southern hemisphere) and P_2 (in the subcritical area, southern hemisphere). The three points are depicted together with their local reference framework (denoted with a corresponding number of primes) where angles of incidence (ϕ_i) and reflection (ϕ_r) are also defined, in the appropriate reference framework.

From P_0 the ray is moving parallel to the y-axis, with an inclination of 45° with respect to the z-axis (common for all reference frameworks), hence $x_1 = x_0$ and $z_1 = -y_1$.

Moreover, P_1 has to belong to the southern hemisphere of the spheroid, yielding

$$y_1^2 = \frac{1 - x_0^2}{1 + \lambda^2} \tag{A 2}$$

with $y_1 > 0$. Then, we prescribe P_2 to lie on the y-axis, $x_2 = 0$, and to be part of the southern hemisphere of the spheroid as well:

$$y_2^2 + \lambda^2 z_2^2 = 1 \tag{A 3}$$

with $z_2 < 0$. The ray connecting P_1 and P_2 forms an angle of 45° with the vertical, therefore it follows that the projection on the horizontal plane of the segment connecting the two points is equivalent in length to the projection on the vertical plane of the same segment. Since the length of this segment is invariant under rotation of the reference framework and equal to $\sqrt{x_0^2 + (y_1 - y_2)^2}$, we can write

$$z_2 = z_1 - \sqrt{x_0^2 + (y_1 - y_2)^2} = -y_1 - \sqrt{x_0^2 + (y_1 - y_2)^2}. \tag{A 4}$$

According to the horizontal refraction law (2.10), a horizontally symmetric subcritical reflection (as the one needed in P_2) occurs when the incident direction in the local reference framework, ϕ_i, satisfies

$$\phi_i = \cos^{-1}(-s) \tag{A 5}$$

where $s = |\nabla H|$ represents the local bottom slope. In that case $\sin\phi_r = \sin\phi_i$, implying $\phi_r = \pi - \phi_i$. Since, as can be seen in figure 24,

$$\phi_{i,2} = \phi_{r,1} - \phi_{i,1}, \tag{A 6}$$

where the second subscript corresponds to the framework of the definition of the angle, a symmetric subcritical reflection will occur in P_2 only if

$$\phi_{r,1} = \cos^{-1}(-s_2) + \phi_{i,1} \tag{A 7}$$

with

$$\phi_{i,1} = \pi/2 - \tan^{-1}(y_1/x_0). \tag{A 8}$$

This implies

$$\left.\begin{aligned} \sin(\phi_{i,1}) &= 1 \Big/ \sqrt{1 + \left(\frac{y_1}{x_0}\right)^2} \\ \cos(\phi_{i,1}) &= 1 \Big/ \sqrt{1 + \left(\frac{x_0}{y_1}\right)^2} \end{aligned}\right\}. \tag{A 9}$$

Knowing that the reflection in P_1 must be supercritical, equation (2.10) reads:

$$\frac{\sin(\phi_{r,1})}{\sin(\phi_{i,1})} = \frac{s_1^2 - 1}{1 + 2s_1\cos(\phi_{i,1}) + s_1^2}. \tag{A 10}$$

Using (A 2), (A 7) and (A 8) and the local bottom slopes:

$$\left.\begin{aligned} s_1 &= \frac{\sqrt{1 - \lambda^2 y_1^2}}{\lambda^2 |y_1|} \\ s_2 &= \frac{y_2}{\lambda^2 |z_2|} \end{aligned}\right\}. \tag{A 11}$$

Equation (A 10) can then be rewritten in terms of point coordinates only, and yields

$$\frac{y_2}{\lambda^2|z_2|} - \frac{y_1}{x_0}\sqrt{1 - \left(\frac{y_2}{\lambda^2|z_2|}\right)^2} = \frac{-1 + \lambda^2(1 - x_0^2)}{1 + \lambda^2(1 - x_0^2)}. \tag{A 12}$$

The last condition relates the position of P_1 to the angle of incidence required at P_2. Indeed x_0 $(= x_1)$ has to satisfy the condition

$$x_0 = \sqrt{x_0^2 + (y_1 - y_2)^2}\,\sin(\cos^{-1}(-s_2)). \tag{A 13}$$

Using that

$$\sin(\cos^{-1}(-s_2)) = \sqrt{1 - s_2^2}, \tag{A 14}$$

it follows that

$$\frac{x_0^2}{(y_2 - y_1)^2} = \frac{\lambda^2}{y_2^2} - (1 + \lambda^2). \tag{A 15}$$

Equations (A 2)–(A 4), (A 12) and (A 15) now form a system in $(x_0, \lambda, y_1, y_2, z_2)$ that can be solved analytically:

$$\begin{cases} x_0 = 1/\sqrt{3} \\ \lambda = 1/\sqrt{2} \\ y_1 = 2/3 \\ y_2 = 1/3 \\ z_2 = -4/3. \end{cases} \tag{A 16}$$

The corresponding eigenfrequency for this closed orbit, following from the value of λ, is $\omega = \sqrt{2/3}$.

Appendix B. Spatial structure of periodic trajectories in the case $\omega^2 < 1/2$

When $\omega^2 < 1/2$ the sphere is transformed into an oblate spheroid, according to (2.9). We have noticed that in this case, if a polygon or star-shaped periodic trajectory exists at a certain frequency $\hat{\omega}$, it crosses the equatorial plane at $P = \{x_{eq}, 0, 0\}$ with x_{eq} given by

$$x_{eq} = \sqrt{\frac{1 - 2\hat{\omega}^2}{1 - \hat{\omega}^2}} \tag{B 1}$$

and with a direction $\phi_{eq} = \pi/2$. Remarkably, the value of the Cartesian coordinate x_{eq} corresponds to the eccentricity ϵ of the stretched spheroid obtained using (2.9). It follows that $\pm\epsilon$ corresponds also to the distance in the (x, z) or (y, z)-plane of the foci of the ellipse from the centre. The full set of parameters needed for the periodic trajectory then immediately follows:

$$\begin{cases} \hat{\omega} \\ \boldsymbol{x}_0 = \{x_{eq}, 0, 0\} \\ \phi_0 = \pi/2 \\ \gamma_0 = \pm 1 \end{cases} \tag{B 2}$$

where the sign of the vertical group velocity will only determine the direction of propagation of the ray.

Moreover, for polygon-shaped orbits, it is also possible to predict a valid set of parameters ω, x_0, ϕ_0 and γ_0 with x_0 part of the boundary and in particular of the critical latitude θ_c. Giving the eigenfrequency $\hat{\omega}$, the distance from the rotation axis r_{θ_c} of the critical latitude θ_c is

$$r_{\theta_c} = \sqrt{1 - \hat{\omega}^2}. \tag{B 3}$$

The launching direction ϕ_0 at the critical latitudes, then, immediately follows according to the number of sides (L) constituting the polygonal top view shape of the orbit. The full set of parameters needed for the periodic trajectory then reads

$$\begin{cases} \hat{\omega} \\ \boldsymbol{x}_0 = \left\{ r_{\theta_c}, 0, \sqrt{1 - r_{\theta_c}^2} \right\} \\ \phi_0 = \pi - \pi/L \\ \gamma_0 = -1. \end{cases} \tag{B 4}$$

Here $z_0 > 0$ and $\gamma_0 < 0$, since we are assuming the launching point is on the northern hemisphere.

Looking at figure 4, it is clear that these simple rules have helped the authors to visualize a larger set of periodic orbits in the low-frequency regime ($\omega^2 < 1/2$) than in the high-frequency regime. However, these rules can only be applied once the geometrical pattern of an orbit (number of vertices, winding number) is known or can be predicted, which enabled the visualization of periodic trajectories only for the polygon and star families, because of their regularity and their monotonic behaviour with frequency (i.e. the number of vertices of the polygon decreases with frequency). The key role played by the critical circles has also been of help.

REFERENCES

ALDRIDGE, K. D. & TOOMRE, A. 1969 Axisymmetric inertial oscillations of a fluid in a rotating spherical container. *J. Fluid Mech.* **37**, 307–323.

ARRAS, P., FLANAGAN, E. E., MORSINK, S. M., SCHENK, A. K., TEUKOLSKY, S. A. & WASSERMAN, I. 2003 Saturation of the *r*-mode instability. *Astrophys. J.* **591**, 1129–1151.

BAINES, P. G. 1971 The reflexion of internal/inertial waves from bumpy surfaces. *J. Fluid Mech.* **46**, 273–292.

BARBOSA AGUIAR, A. C., READ, P. L., WORDSWORTH, R. D., SALTER, T. & HIRO YAMAZAKI, Y. 2010 A laboratory model of Saturn's North Polar Hexagon. *Icarus* **206** (2), 755–763.

BARCILON, V. 1968 Axi-symmetric inertial oscillations of a rotating ring of fluid. *Mathematika* **93**, 93–102.

BARUTEAU, C. & RIEUTORD, M. 2013 Inertial waves in a differentially rotating spherical shell. *J. Fluid Mech.* **719**, 47–81.

BERRY, M. V. 1981 Regularity and chaos in classical mechanics, illustrated by the three deformations of a circular 'billiad'. *Eur. J. Phys.* **2**, 91–102.

BERRY, M. V. 1987 Quantum chaology. *Proc. R. Soc. Lond.* A **413**, 42–45.

BROUTMAN, D., ROTTMAN, J. W. & ECKERMANN, S. D. 2004 Ray methods for internal waves in the atmosphere and ocean. *Annu. Rev. Fluid Mech.* **36** (1), 233–253.

BRYAN, G. H. 1889 The waves on a rotating liquid spheroid of finite ellipticity. *Proc. R. Soc. Lond.* **45**, 42–45.

CARTAN, M. E. 1922 Sur les petites oscillations d'une masse de fluide. *Bull. Sci. Math.* **46**, 317–369.

DINTRANS, B. & OUYED, R. 2001 On Jupiter's inertial mode oscillations. *Astron. Astrophys.* **375** (L47), 1–4.

DINTRANS, B., RIEUTORD, M. & VALDETTARO, L. 1999 Gravito-inertial waves in a rotating stratified sphere or spherical shell. *J. Fluid Mech.* **398**, 271–297.

DRIJFHOUT, S. & MAAS, L. R. M. 2007 Impact of channel geometry and rotation on the trapping of internal tides. *J. Phys. Oceanogr.* **37** (11), 2740–2763.

ECKART, C. 1960 *Hydrodynamics of Oceans and Atmospheres*. Pergamon.

ERIKSEN, C. C. 1985 Implications of ocean bottom reflection for internal wave spectra and mixing. *J. Phys. Oceanogr.* (15), 1145–1156.

FAVIER, B., BARKER, A. J., BARUTEAU, C. & OGILVIE, G. I. 2014 Nonlinear evolution of tidally forced inertial waves in rotating fluid bodies. *Mon. Not. R. Astron. Soc.* **439** (1), 845–860.

GILBERT, D. & GARRETT, C. 1989 Implications for ocean mixing of internal wave scattering off irregular topography. *J. Phys. Oceanogr.* (19), 1716–1729.

GODFREY, D. A. 1988 A hexagonal feature around Saturn's north pole. *Icarus* **76** (2), 335–356.

GÖRTLER, H. 1943 Uber eine schwingungserscheinung in flussigkeiten mit stabiler dichteschichtung. *Z. Angew. Math. Mech.* **23**, 65–71.

GREENSPAN, H. P. 1968 *The Theory of Rotating Fluids*. Cambridge University Press.

GUTZWILLER, M. C. 1990 *Chaos in Classical and Quantum Mechanics*. Springer.

HARLANDER, U. & MAAS, L. R. M. 2006 Characteristics and energy rays of equatorially trapped, zonally symmetric internal waves. *Meteorol. Z.* **15** (4), 439–450.

HARLANDER, U. & MAAS, L. R. M. 2007 Internal boundary layers in a well-mixed equatorial atmosphere/ocean. *Dyn. Atmos. Oceans* **44** (1), 1–28.

HAZEWINKEL, J., GRISOUARD, N. & DALZIEL, S. B. 2010 Comparison of laboratory and numerically observed scalar fields of an internal wave attractor. *Eur. J. Mech. (*B*/Fluids)* **30**, 51–56.

HAZEWINKEL, J., MAAS, L. R. M. & DALZIEL, S. B. 2011 Tomographic reconstruction of internal wave patterns in a paraboloid. *Exp. Fluids* **50**, 247–258.

HAZEWINKEL, J., VAN BREEVOORT, P., DALZIEL, S. B. & MAAS, L. R. M. 2008 Observations on the wavenumber spectrum and evolution of an internal wave attractor. *J. Fluid Mech.* **598**, 373–382.

HELLER, E. J. 1984 Bound-state eigenfunctions of classically chaotic Hamiltonian systems: scars of periodic orbits. *Phys. Rev. Lett.* **53**, 1515–1518.

HØILAND, E. 1962 Discussion of a hyperbolic equation relating to inertia and gravitational fluid oscillations. *Geophys. Publ.* **26**, 211–227.

HOLLERBACH, R., FUTTERER, B., MORE, T. & EGBERS, C. 2004 Instabilities of the Stewartson layer part 2. Supercritical mode transitions. *Theor. Comput. Fluid Dyn.* **18**, 197–204.

HUGHES, B. 1964 Effect of rotation on internal gravity waves. *Nature* **201** (4921), 798–801.

IVANOV, P. B. & PAPALOIZOU, J. C. B. 2010 Inertial waves in rotating bodies: a WKBJ formalism for inertial modes and a comparison with numerical results. *Mon. Not. R. Astron. Soc.* **407** (3), 1609–1630.

JOHN, F. 1941 The Dirichlet problem for hyperbolic equation. *Am. J. Maths* **63**, 141–154.

LORD KELVIN, 1877 On the precessional motion of a liquid. *Nature* **15**, 297–298.

LORD KELVIN, 1880*a* On an experimental illustration of minimum energy. *Nature* **23**, 69–70.

LORD KELVIN, 1880*b* Vibrations of a columnar vortex. *Phil. Mag.* (10), 155–168.

KOCH, S., HARLANDER, U., EGBERS, C. & HOLLERBACH, R. 2013 Inertial waves in a spherical shell induced by librations of the inner sphere: experimental and numerical results. *Fluid Dyn. Res.* **45** (3), 35504.

KUDLICK, M. D. 1966 *On Transient Motions in a Contained Rotating Fluid*. PhD thesis, Math. Dept., MIT.

KUDROLLI, A., ABRAHAM, M. C. & GOLLUB, J. P. 2001 Scarred patterns in surface waves. *Phys. Rev.* E **63** (2), 1–8.

LE BARS, M., LE DIZÈS, S. & LE GAL, P. 2007 Coriolis effects on the elliptical instability in cylindrical and spherical rotating containers. *J. Fluid Mech.* **585**, 323–342.

LEWIS, B. M. & HAWKINS, H. F. 1982 Polygonal eye walls and rainbands in hurricans. *Bull. Am. Meteorol. Soc.* **63** (11), 1294–1300.

LOCKITCH, K. H. & FRIEDMAN, J. L. 1999 Where are the *r*-modes of isentropic stars? *Astrophys. J.* **521**, 764–788.

MAAS, L. R. M. 2003 On the amphidromic structure of inertial waves in a rectangular parallelepiped. *Fluid Dyn. Res.* **373**, 373–401.

MAAS, L. R. M. 2005 Wave attractors: linear yet nonlinear. *Intl J. Bifurcation Chaos* **15** (9), 2757–2782.

MAAS, L. R. M., BENIELLI, D., SOMMERIA, J. & LAM, F.-P. A. 1997 Observation of an internal wave attractor in a confined, stably stratified fluid. *Nature* **388**, 557–561.

MAAS, L. R. M. & LAM, F.-P. A. 1995 Geometric focusing of internal waves. *J. Fluid Mech.* **300**, 1–41.

MANDERS, A. M. M. & MAAS, L. R. M. 2004 On the three-dimensional structure of the inertial wavefield in a rectangular basin with one sloping boundary. *Fluid Dyn. Res.* **35**, 1–21.

MÜNNICH, M. 1996 The influence of bottom topography on internal seiches in stratified media. *Dyn. Atmos. Oceans* **23**, 257–266.

NÖCKEL, J. U. 1997 Resonances in nonintegrable open systems. PhD thesis, Yale University.

NÖCKEL, J. U., STONE, A. D., CHEN, G., GROSSMAN, H. L. & CHANG, R. K. 1996 Directional emission from asymmetric resonant cavities. *Opt. Lett.* **21**, 1609–1611.

NOIR, J., BRITO, D., ALDRIDGE, K. & CARDIN, P. 2001 Experimental evidence of inertial waves in a precessing spheroidal cavity. *Geophys. Res. Lett.* **28** (19), 3785.

NURIJANYAN, S., BOKHOVE, O. & MAAS, L. R. M. 2013 A new semi-analytical solution for inertial waves in a rectangular parallelepiped. *Phys. Fluids* **25** (12), 126601.

OGILVIE, G. I. 2005 Wave attractors and the asymptotic dissipation rate of tidal disturbances. *J. Fluid Mech.* **543**, 19–44.

OGILVIE, G. I. & LIN, D. N. C. 2004 Tidal dissipation in rotating giant planets. *Astrophys. J.* **610**, 477–509.

PHILLIPS, O. M. 1963 Energy transfer in rotating fluids by reflection of inertial waves. *Phys. Fluids* **6**, 513–520.

RABITTI, A. & MAAS, L. R. M. 2013 Meridional trapping and zonal propagation of inertial waves in a rotating fluid shell. *J. Fluid Mech.* **729**, 445–470.

RIEUTORD, M. 1991 Linear theory of rotating fluids using spherical harmonics part II, time-periodic flows. *Geophys. Astrophys. Fluid Dyn.* **59**, 185–208.

RIEUTORD, M., GEORGEOT, B. & VALDETTARO, L. 2000 Wave attractors in rotating fluids: a paradigm for ill-posed Cauchy problems. *Phys. Rev. Lett.* **85** (20), 4277–4280.

RIEUTORD, M., GEORGEOT, B. & VALDETTARO, L. 2001 Inertial waves in a rotating spherical shell: attractors and asymptotic spectrum. *J. Fluid Mech.* **435**, 103–144.

RIEUTORD, M., VALDETTARO, L. & GEORGEOT, B. 2002 Analysis of singular inertial modes in a spherical shell: the slender toroidal shell model. *J. Fluid Mech.* **463**, 345–360.

SCOLAN, H., ERMANYUK, E. & DAUXOIS, T. 2013 Nonlinear fate of internal wave attractors. *Phys. Rev. Lett.* **110** (23), 234501.

STEWARTSON, K. & RICKARD, J. A. 1969 Pathological oscillations of a rotating fluid. *J. Fluid Mech.* **35**, 759–773.

VAN HAREN, H. & GOSTIAUX, L. 2012 Energy release through internal wave breaking. *Oceanography* **25** (2), 124–131.

WHITHAM, G. B. 1960 A note on group velocity. *J. Fluid Mech.* **9**, 347–352.

WHITHAM, G. B. 1974 *Linear and Non Linear Waves*. John Wiley & Sons.

WU, Y. 2005*a* Origin of tidal dissipation in Jupiter. I. Properties of inertial modes. *Astrophys. J.* **635**, 674–687.

WU, Y. 2005*b* Origin of tidal dissipation in Jupiter. II. The value of *Q*. *Astrophys. J.* **13**, 688–710.

WUNSCH, C. & FERRARI, R. 2004 Vertical mixing, energy, and the general circulation of the oceans. *Annu. Rev. Fluid Mech.* **36** (1), 281–314.

ZHANG, K., CHAN, K. H., LIAO, X. & AURNOU, J. M. 2013 The non-resonant response of fluid in a rapidly rotating sphere undergoing longitudinal libration. *J. Fluid Mech.* **720**, 212–235.

ZHANG, K., EARNSAHW, P., LIAO, X. & BUSSE, F. H. 2001 On inertial waves in a rotating fluid sphere. *J. Fluid Mech.* **437**, 103–119.